2013

1891 AD Submarine Eruptive Processes and Geochemical Studies of Floating Scoria at Foerstner Volcano, Pantelleria

Joshua Kelly
University of Rhode Island, j_kelly@my.uri.edu

1891 AD SUBMARINE ERUPTIVE PROCESSES AND GEOCHEMICAL STUDIES OF FLOATING SCORIA AT FOERSTNER VOLCANO, PANTELLERIA

BY

JOSHUA KELLY

A THESIS SUBMITTED IN PARTIAL FULFILLMENT OF THE

REQUIREMENTS FOR THE DEGREE OF

MASTER OF SCIENCE

IN

OCEANOGRAPHY

UNIVERSITY OF RHODE ISLAND

2013

MASTER OF SCIENCE THESIS

OF

JOSHUA KELLY

APPROVED:

Thesis Committee:

Major Professor: Steve Carey

Chris Roman

Dawn Cardace

Nasser H. Zawia
DEAN OF THE GRADUATE SCHOOL

UNIVERSITY OF RHODE ISLAND
2013

Abstract

On October 17, 1891 a submarine eruption occurred at Foerstner volcano in the Straits of Sicily 4 km northwest of the island of Pantelleria, Italy. The eruption produced floating scoria bombs, or balloons, that discharged gas at the surface and eventually sank to the seafloor. Activity occurred for a period of one week from an eruptive vent located within the Pantelleria Rift at a water depth of 250 m.

Remotely Operated Vehicle (ROV) video footage and high resolution multibeam mapping of the Foerstner vent site was used to create a geologic map of the 1891 AD deposits and conduct the first detailed study of the source area associated with this unusual type of submarine volcanism. The main Foerstner vent consists of two overlapping circular mounds with a total volume of 6.3×10^5 m^3 and relief of 60 m. It is dominantly constructed of clastic scoriaceous deposits with some interbedded effusive pillow flow deposits. Petrographic and geochemical analyses of Foerstner samples by X-ray fluorescence and inductively coupled plasma mass spectrometry reveal that the majority of the deposits are highly to extremely vesicular, hypocrystalline tephrite basanite scoria that display porphyritic, hyaloophitic, and vitrophyric textures. An intact scoria balloon recovered from the seafloor consists of an interior gas cavity surrounded by a thin lava shell comprised of two distinct layers; a thin, oxidized quenched crust surrounding the exterior of the balloon and a dark grey, tachylite layer lying beneath it. Ostwald ripening is determined to be the dominant bubble growth mechanism of four representative Foerstner scoria samples as determined by vesicle size distributions.

Characterization of the diversity of deposit facies observed at Foerstner in conjunction with quantitative rock texture analysis indicates that Strombolian-like activity is the most likely mechanism for the formation of buoyant scoria bombs. The deposit facies observed at the main Foerstner vent are very similar to those produced by other known submarine Strombolian eruptions (short pillow flow lobes, large scoriaceous clasts, spatter-like vent facies). Balloons were likely formed from the rapid cooling of extremely vesicular magma fragments as a result of a gas-rich frothy magma source. The exterior of these fragments hyperquenched forming a vesicular glassy shell that acted as an insulating layer preventing magmatic gas in its interior from escaping and thus allowing flotation as densities reached less than 1000 kg/m^3. We believe that lava balloon eruptions are more common than previously thought, as the eruptive conditions required to generate these products are likely to be present in a variety of submarine volcanic environments. Additionally, the facies relationships observed at Foerstner may be used as a paleoenvironmental indicator for modern and ancient basaltic shallow submarine eruptions because of the relatively narrow depth range over which they likely occur (200-400 m).

Acknowledgements

This work was supported financially by the National Science Foundation, NOAA Ocean Exploration Program, and the Ocean Exploration Trust.

My first and foremost gratitude lies with my advisor, Steve Carey, for pointing me in the direction of this topic from day one. His endless amounts of support and enthusiasm are, in large part, responsible for my graduating in a timely manner. He has shown time and time again that not only his graduate students but also all students are of his utmost importance. I am extremely grateful for his patience and open-door policy that has made my time as a graduate student extremely enjoyable and fulfilling.

I want to give a huge thank you to Marion Lytle who spent many hours helping me with sample preparation for and using the ICP-MS and the data reduction. Another enthusiastic thank you to Chris Roman who was essential in creating the bathymetric and geologic maps that are published in this thesis as well as showing a great amount of patience when helping me with MATLAB.

I would like to thank Katy Croff Bell and the rest of the science team and crew aboard the *E/V Nautilus* in Fall 2011 for making this study possible and allowing me to participate in oceanographic cruises. Further thanks to Dr. Robert Ballard and the Ocean Exploration Trust and the GSO Alumni Association for their extreme generosity, which allowed me to present my research in San Francisco at the AGU meeting.

I would also like to thank my other committee member, Dawn Cardace, for her helpful comments as well as my committee chair, Tom Boving, for his willingness to assume the responsibility. I would also like to recognize Maryann Scholl and the

Office of Marine Programs who provided me the opportunity to be an Outreach Scientist.

Finally, I would not be where I am today if it weren't for my family. The love, care, and guidance they have provided me is the backbone for all I have done and will ever do in my life. Thank you guys.

Preface

This thesis is an integrated volcanologic and geochemical analysis of the 1891 AD eruption of Foerstner submarine volcano in the Straits of Sicily. An abstract pertaining to the structure and deposit facies of this vent was presented at the American Geophysical Union (AGU) annual conference in 2012 under the title "1891 eruption of Foerstner volcano (Pantelleria, Sicily): insights into the vent structure of basaltic balloon eruptions".

This thesis is presented in manuscript format and has been completed with the intention of submission to the Bulletin of Volcanology.

Table of Contents

List of Tables

List of Figures

1891 AD submarine eruptive processes and geochemical studies of floating scoria at Foerstner Volcano, Pantelleria

by

J. Kelly[1], S. Carey[1], K. L. Croff Bell[2], C. Roman[1], M. Rosi[3], M. Marani[4], M. Pistolesi[4], E. Baker[5]

is formatted for submission to

Bulletin of Volcanology

[1]Graduate School of Oceanography, The University of Rhode Island, Narragansett, RI 02882.

[2]Ocean Exploration Trust, Narragansett, RI 02882

[3]Earth Sciences, University of Pisa, Pisa, Italy

[4]Institute of Marine Science, National Research Council, Bologna, Italy

[5]Pacific Marine Environmental Laboratory, Seattle, WA 98115

Introduction

Shallow submarine volcanism that produces floating basaltic scoria bombs is one of the most peculiar and rarely observed eruption styles on Earth (Kueppers et al., 2012). Rapid degassing of mafic magma at shallow depths (< 400 m) can lead to highly vesicular, extremely low-density volcanic products. Owing to their morphology and behavior, the floating scoria bombs have been termed "lava balloons" (Gaspar et al., 2003). Eruptive conditions that generate these products are not well understood due to their rare occurrence and paucity of direct submarine observations. Previous investigations only recovered samples while they were still floating on the sea surface and no attempts to describe the vent site and/or the distribution of the bombs after sinking have been made. This has led to debate as to the style of submarine eruptions that produces these unique deposits (e.g. Gaspar et al., 2003). There have been only five cases where floating basaltic bombs have been observed during submarine eruptions: the recent 2011-2012 eruption of El Hierro, Canary Islands, Spain (Troll et al., 2012), a 1993 eruption near Socorro Island, Mexico (Siebe et al., 1995), a 1877 eruption west of the island of Hawai'i, USA (Moore et al., 1985), a 1998-2001 eruptive episode of the Serreta Submarine Ridge northwest of Terceira Island, Azores (Gaspar et al., 2003; Kueppers et al., 2012), and the 1891 eruption of Foerstner volcano northwest of Pantelleria island (Washington, 1909: Butler, 1892). The Foerstner eruption was the most recent volcanic activity in the Straits of Sicily. It occurred within the Pantelleria graben, a large, tectonic depression, 90 km long and 30 km wide, that has a general NW-SE orientation and is bounded by very steep normal faults (Civile at al, 2010). Like other balloon eruptions, it produced ellipsoidal,

scoriaceous bombs that rose intact through the water column and floated on the surface of the sea before becoming saturated with seawater and sinking (Washington, 1909, Butler, 1892). Many were greater than 1 m in diameter and extremely vesicular with individual vesicles reaching up to decimeters in size.

In this study, we report on remotely operated vehicle (ROV) explorations of the vent area of the 1891 Foerstner eruption carried out during cruise NA-018 of the E/V *Nautilus*. This is the first detailed study of the vent site of a basaltic balloon eruption and a geologic map of the volcanic products has been created using a high-resolution mapping and photographic survey of the area. Geochemical and mineralogical analyses of samples collected by the ROV provide information about magma composition, viscosity, and crystal content of the 1891 products. The MATLAB-based program, FOAMS, was used to investigate the degassing processes of the basaltic balloons based on imaging of bubble size distributions. We compare the Foerstner balloons to the products of other basaltic balloon events and develop an eruption model to describe the vent facies and processes that led to the formation of the balloons during the 1891 eruption. The results from this well constrained example provide an important basis for the facies interpretation of ancient highly vesicular submarine basaltic sequences (e.g. Simpson and McPhie, 2001).

Geologic Setting

The Straits of Sicily is located in the northern part of the African continental plate called the Pelagian block (Figure 1, Burollet et al., 1978). It is bounded by the Skerki bank to the west and the Malta escarpment to the east and is very shallow

(averaging 350 m depth), except in three NW-trending depressions (Civile et al., 2010). The Sicily Channel has been affected by Late Miocene-Early Pliocene continental rifting (Civile et al., 2008), which produced several geologic features. The rifting created the Pantelleria, Malta, and Linosa tectonic depressions, which reach depths of 1350, 1580, and 1720m and are bounded by NW-SE trending normal faults (Calanchi et al., 1989; Civile et al., 2008). It also created two volcanic islands (Pantelleria and Linosa) and a series of magmatic seamounts located in the Adventure Plateau, Graham and Nameless banks (Peccerillo, 2005; Rotolo et al., 2006). The rifting also led to a thinning of the continental crust beneath the troughs up to about 17 km along the Pantelleria graben axis (Civile et al., 2008). The rifting has been interpreted as a result of mantle convections developed during the roll-back of the African lithosphere slab beneath the Tyrrhenian basin (Argnani, 1990). The tectonic depressions have also been interpreted as large pull-apart basins involving deep crustal levels, formed within a large wrench zone in front of the Africa-Europe collisional belt (Cello et al., 1985). The rifting may also be related to the NE-directed displacement of Sicily away from the African continent (Illies, 1981). These diverse interpretations show that the tectonic mechanisms responsible for the Sicily Channel rift zone are still not well understood.

Pantelleria Island has a surface area of 83 km^2 and represents the largest extent of an emerged composite volcano in the Sicily Channel, rising from a depth of 1300 m to 830 m above sea level (Civile et al., 2010; Martorelli et al., 2011). The island is composed wholly of peralkaline trachytes and rhyolites (pantellerites) (Civetta et al., 1988) produced by Late Quaternary volcanic activity. The activity was mainly

explosive and characterized by caldera collapses producing large volumes of ignimbrites and pyroclastics (Civetta et al., 1984, 1988). Pantelleria is characterized by notable volcano-tectonic features such as caldera rims, emission centers, and dike swarms, most significant of which are two large calderas that developed on the southeastern part of the island (Civile et al, 2008). High-resolution mapping of the Pantelleria submarine flanks shows numerous small volcanic cones concentrated to the NW of the island (Bosman et al., 2007). Seismic profiles and regional magnetic anomalies indicates that volcanic bodies with a clear magnetic signature are exposed at the seafloor as far as 37 km northwest and southeast of Pantelleria, with their elongation consistent with the orientation of the rift (Calanchi et al., 1988). Volcanic bodies southeast of the island are buried beneath undisturbed Upper Pliocene-Quaternary sediments, suggesting major volcanic activity in the early stage of the graben development, which partly filled the rift floor (Calanchi et al., 1988). The bodies located northwest of the island are probably related to volcanic activity associated with the development of the Pantelleria Rift (Calanchi et al., 1988). Seismic activity of the Sicily Channel is characterized by shallow (<25 km), low magnitude (2 to 4) events (Civile et al., 2008). Seismicity is notably absent along the Pantelleria graben, while some earthquakes have been recorded north of Pantelleria.

In the Sicily Channel, volcanic activity was concentrated mainly on the islands of Pantelleria and Linosa during the Pleistocene. Minor submarine volcanism began during the early Pliocene and lasted until 110 years ago, mainly occurring in Adventure plateau and in Graham and Nameless Banks (Corti et al., 2006; Rotolo et al., 2006). The oldest products have been found in a volcanic seamount located east of

Nameless Bank, where dredged samples gave a K-Ar age of 9.5 Ma (Beccaluva et al., 1981). The most recent activity occurred during the nineteenth century, most notably in the Graham Bank in 1831 and Foerstner volcano in 1891, the most recent eruption (Washington, 1909). Additional eruptions occurred in 1801, 1845, 1846, and 1863 but were not observed because they did not give rise to a permanent subaerial island due to short periods of activity (Washington, 1909).

Historical Accounts of the 1891 Foerstner Submarine Eruption

In 1890, many premonitory signals to an eruption were detected on Pantelleria, as summarized by A. Ricco (Butler, 1892). These signals included increased fumarolic activity causing damage to vineyards, increased earthquake activity, and uplift of the island's north coast due to increased tectonic activity (Butler, 1892). On October 14-15, 1891 (three days before the eruption began), stronger earthquakes were accompanied by the drying up of hot springs and a further rise of the north coast (totaling 80 cm), which resulted in surface cracks (Washington, 1909; Butler, 1892). Large amplitude earthquakes preceded the beginning of the eruption on the morning of October 17, after which all earthquake activity ceased (Washington, 1909).

The 1891 eruption of Foerstner volcano lasted only a week and was not described by any scientific observer. Descriptions of the eruption have been derived from the testimony of fishermen, most notably A. Ricco, whose account was translated by G. W. Butler in 1892 and provides the basis for the description that follows (Washington, 1909). The first signs of the eruption were deep rumblings and columns of "smoke" protruding from the sea surface 4 km west of the town of Pantelleria at the northwest

end of the island. Black, subspherical, scoriaceous bombs up to 1 m in diameter were seen rising to the surface along a NE-SW trending line about 850-1000 m long, initially thought to have been produced by fissure activity (Figure 2). Some of the bombs were still degassing at the surface and as a result, were propelled laterally by horizontal steam jets. Some were thrown up to 20 m in the air as a result of rapid degassing. Bombs collected at the surface were still at very high temperature inside (at least 415º C as indicated by fusion of Zn) and one bomb was noted as being incandescent. After the degassing episodes had ceased, the scoria balloons sank as a result of seawater saturation. Some claim that an ephemeral island was formed (including Foerstner himself), but both Ricco and Butler explicitly deny this suggestion. The highest water temperature recorded at the eruption site as 1.5º C above the ambient temperature. It was noted that there was a strong smell "as of gunpowder" at the site, which was most likely H_2S and SO_2 gas emissions. The eruption ceased on October 25, 1891.

Methodology

The suspected vent site of the 1891 Foerstner eruption (Bosman et al., 2007) was explored using the remotely operated vehicle (ROV) *Hercules* during cruise NA018 of the E/V *Nautilus* in October 2011 (Figure 3). A BlueView 1350 kHz 90-degree multi-beam echo sounder was used to generate a high-resolution bathymetric map of the area (~250 x 250 m) based on a survey conducted at an altitude of 8-10 m above the seafloor. Data were processed and gridded to 20 cm cell size for water depths of 250-360 m.

Scoria and lava flow samples were collected at 42 sites at or in close proximity to the submarine vent site using the ROV. Ten samples that encompass the major clast types observed at the vent site were selected for petrographic and geochemical analyses. Bulk samples were cleaned in de-ionized (DI) water, sonicated for 30 minutes to remove foreign particles, rinsed in DI water again, and then dried for 48 hours at 100° C. Powdered whole rocks were analyzed for major elements by X-ray fluorescence (XRF) using the standard BHVO-2 at the Ronald B. Gilmore X-ray Fluorescence Laboratory, University of Massachusetts, Amherst. Trace element compositions in the same powders were analyzed using the New Wave 213 nm Nd-YAG laser, attached to a Thermo X-Series II ICP-MS at Dr. Katie Kelley's lab at URI's Graduate School of Oceanography (GSO) in Narragansett, RI following the methods of Kelley et al. (2003). Standards used were: JB-3, BHVO-1, DNC-1, W-2, and EN026 10D-3. Reproductibility of replicate analyses is <2% rsd. Petrographic descriptions of these samples were completed using a Zeiss Axioscopt petrographic microscope in Dr. Steven Carey's lab at GSO.

Characterization of bubble textures in vesicular samples was carried out following the methods of Shea et al. (2010). Thin sections made from selected samples were imaged using a petrographic microscope and a scanning electron microscope (SEM), using 5x-100x magnifications to image a range of vesicle sizes between 10 μm and 1.58 mm. SEM imaging was done using a JEOL JSM-5900LV SEM at Mike Platek's lab at the University of Rhode Island, Kingston, RI. The nested images were used to derive vesicle volume distributions via the FOAMS program (Shea et al. 2010).

A geologic map of Foerstner volcano was created using high definition video footage recorded by *Hercules.* A total of 40 hours of video footage of the Foerstner vent site and surrounding area was recorded during dives H1205, H1206, and H1207. Preliminary viewing of the video was used to identify 17 different facies of volcaniclastic and effusive deposits. The video footage was then systematically viewed and facies type was recorded at one minute intervals and linked to the ROV navigation tracks. The map was created using Adobe Illustrator®.

Mineralogy and Petrography

All samples from the vent area of Foerstner volcano are plagioclase-olivine-phyric basanite. The majority are hypocrystalline and display porphyritic, hyaloophitic, and vitrophyric textures. Plagioclase is present mostly as acicular with some tabular and few equant microphenocrysts and phenocrysts (0.03-1.85 mm) as well as microlites. Olivine is mainly present as microlites, but with some euhedral to subhedral microphenocrysts and few phenocrysts (0.03-0.85 mm) that contain melt inclusions. Olivine also occurs within aggregates (glomerocrysts) in some samples. Subhedral augite is the least commonly found phenocryst.

The groundmass of the samples consists of sideromelane, tachylite, or a mixture of both. Tachylite is cryptocrystalline glass and is the result of confined conditions of crystallization, controlled by local enrichment-depletion of elements adjacent to precipitating minerals (Taddeucci et al. 2004). Tachylite is nearly opaque as it contains abundant microlites leading to an optical isotropy similar to magnetite (Morris et al., 1990). Vesicularity descriptions used in this study are adopted from

Houghton and Wilson (1989) and are as follows: 0-5% non-vesicular, 5-20% incipiently vesicular, 20-40% poorly vesicular, 40-60% moderately vesicular, 60-80% highly vesicular, >80% extremely vesicular. Most of the samples from the Foerstner vent area are highly to extremely vesicular.

Foerstner samples containing sideromelane groundmass are typically much more vesicular than those that have tachylite. Wholly sideromelane samples (NA018-20, 23, 24, 27, 32, and 33) range from highly to extremely vesicular (Figure 4a) compared to wholly tachylite samples (NA018-21, 26, 29, 30, and 31), which are only moderately vesicular (Figure 4b). The rest of the Foerstner samples (NA018-17, 19, and 22) contain both types of glassy groundmass and they gradually transition from one to the other, forming a heterogeneous mixture of the two (Figure 4c). Vesicles are typically fewer but larger in sideromelane samples and irregular in shape due to extensive coalescence.

Sample NA018-025 is unlike all other samples recovered from the Foerstner vent area. It is a moderately vesicular (40%), hypocrystalline, plagioclase-olivine basalt with micritic groundmass and displays porphyritic and hyalopilitic textures (Figure 4d). Plagioclase varies widely in size from microlites to very large acicular and some tabular phenocrysts (0.03-3.4 mm). Olivine is present in the form of microlites and euhedral to subhedral phenocrysts with one anomalously large phenocryst being 2.8 x 1.3 mm in size. The groundmass is much different from the other samples in that it is a mixture of plagioclase microlites and glass.

Whole-rock and Trace Element Compositions

Ten samples were chosen for chemical analyses based on the location and lithology of the submarine deposits (Table 1). Samples analyzed were from the main vent of Foerstner (NA018-019, 021, 022, 023, 026), 125 m south of Foerstner (NA018-025), a northern, deeper vent (NA018-027), in the saddle region between Foerstner and a large seamount to the west (NA018-030), and at the summit of the western seamount (NA018-032, 033) (Table 1). All scoria samples are classified as tephrite basanite according to IUGS classification, occupying a narrow range in SiO_2 abundance from 43.9-44.9 wt% (Figure 5ab, Table 2). Sample NA018-025 to the south of Foerstner is more evolved than the rest of the Foerstner deposits with SiO_2 content of 47.0 wt%.

Washington (1909) carried out the only other chemical analyses of Foerstner scoria deposits. Samples analyzed from the Foerstner vent site in this study are similar in composition to those of Washington (1909), although slightly less evolved (Figure 5a). Low abundances of SiO_2 (~44 wt%), MgO (~5.5 wt%), and alkalis (~4.5 wt%) are common between both analyses as well as the abundance of CaO. Discrepancies arise when comparing Al_2O_3, P_2O_5, and TiO_2. The content of Al_2O_3 is higher in samples from this study (1.7 wt%), while there is 2.1 wt% and 0.5 wt% more TiO_2 and P_2O_5 in Washington's samples. Some of the discrepancies may reflect true compositional differences but they more likely represent interlaboratory differences in techniques used for the analyses that span more than 100 years.

Samples from Foerstner are typically less evolved than samples taken from other nearby volcanic centers in the Straits of Sicily, which are basalt and trachy-

basalt (Figure 5a) (Calanchi et al, 1989). An exception are samples from Nameless and Tetide Banks that are less evolved when compared to Foerstner and plot near the boundary of tephrite basanite-foidite and tephrite basanite-picro-basalt (Figure 5a) (Calanchi et al., 1989).

Whole-rock chemical analyses of the Foerstner samples were compared with all other known submarine lava balloon deposits. Chemical data plotted on the IUGS TAS diagram confirms that each of the four lava balloon deposits are classified as four different types of volcanic rock: Foerstner – tephrite basanite (this study), Socorro – trachy-basalt (Siebe et al., 1995), Hawaii – basaltic andesite (Moore et al., 1985), Azores – basalt (Gaspar et al., 2003) (Figure 5b). There does not appear to be a strong correlation between the composition of magma and the ability to produce lava balloons during eruption, although it is noted that most basaltic balloon eruptions tend to be more alkalic in nature.

The Foerstner basanites show very similar enrichment in the rare earth elements relative to chondrites, with light rare earth elements (LREE) being strongly enriched relative to the heavy rare earth elements (HREE) (Figure 6, Table 3). Following the methods of Peace and Norry (1979), trace elements of the basanites are plotted on the Zr/Y-Zr tectonic discrimination diagram (Figure 7, Table 4). According to this diagram, the high Zr-Y Foerstner samples plot in the within-plate (oceanic island) volcanic province domain. Mid-ocean ridge-normalized (N-MORB) trace element patterns were plotted following the methods of Pearce (1983). Trace element patterns show most incompatible elements are enriched relative to MORB as well as significant enrichment of Ta and Nb (Figure 8) (Pearce, 1983). These patterns are

indicative of intra-continental plate basalts and agree with the REE results. Sample NA018-025 shows anomalous geochemical patterns relative to the rest of the Foerstner samples. It is significantly less enriched in rare earth and trace elements suggesting that it originated from a different magmatic source.

Vent Structure and Deposit Facies

A bathymetric map of the suspected Foerstner vent site was created using high resolution ROV surveys and shows that the volcanic edifice has a slight elliptical shape formed by the overlapping of two circular mounds (Figure 9). In plan view, the vent area has a maximum basal diameter of about 200 m and a relief of 60 m from 250-310 m below sea level corresponding to an approximate total edifice volume of 6.28×10^5 m^3. There is a topographic high located at a depth of 250 m at the SW end of the area and another at a depth of 260 m with a narrow saddle region at 285 m separating the two peaks. Several linear ridges emanate radially towards the northwest and west from the large southwest mound. Bathymetric surveying revealed another smaller vent 100 m to the northwest with a diameter of <50 m at a depth of 360 m (Figure 10). The morphology of this area is more irregular with numerous high relief flow lobes.

The distribution of 17 different facies of volcaniclastic and effusive deposits at Foerstner vent and surrounding area was mapped out based on visual observations of high-definition ROV video footage (Figure 11). The summit of Foerstner (250 m) is dominantly covered by spatter-like deposits that form characteristic spires up to 1 m in height (Figure 12). The flanks of the vent are nearly completely covered by

fragmental pyroclastic deposits. These include scoria bomb beds, which are thick, clast-supported beds of coarse scoria bombs, abundant on the SW flank of the edifice (Figure 13). The abundance of scoria bombs varies on the rest of the vent surface and three different facies were used to distinguish the amount of bombs in a particular area with pelagic or volcanic sediment occupying interstitial space. The NW flank of Foerstner consists of common bombs (25-50%) and sediment with two notable scoria flow lobes found close to the summit. The NE flank is mainly covered by scoria bombs interbedded with pillow and scoria flow lobes. A notably sharp contact between these clastic deposits and pelagic sediment was commonly observed around the base of the edifice. All of the volcanic deposits observed at the main vent had little to no sediment cover. A transit to the south of the main vent revealed a rapid transition from common bombs to fine grained, pelagic sediment. Small groupings of common scoria bombs were discovered approximately 100 m south of the vent. A pillow flow outcrop with significant sediment cover was observed at the southern-most extent of the ROV transit.

A smaller mound was discovered 100 m NW of Foerstner during bathymetric surveying. The edifice has a maximum basal diameter of <50 m and little relief between 350 and 360 m. The amount of fragmental deposits in this area is less than that of the main vent, with the highest abundance of scoria bombs only occupying 25-50% of the W flank. In contrast to the main vent, this smaller vent is dominated by abundant pillow lava flows although the summit does exhibit some spatter-like deposits (Figure 14).

Sunken scoria balloons produced by the 1891 eruption were discovered in a linear transect 300-500 m NW of the main vent. The balloons produced a characteristic crater upon impacting the seafloor, providing evidence that the bombs were at one point floating on the surface (Figure 15). Some of the balloons collapsed in on themselves as a result of their extreme vesiculation and poor internal strength. The balloons varied from 0.5 to 2.2 m in diameter based on rough measurements using *Hercules'* laser calibration dots. While searching for the sunken balloons, two very small vents were discovered northwest of the small mound. Each of these vents is constructed of a single scoria flow lobe indicating extremely brief effusive activity (Figure 16).

Textural Characterization of Foerstner 1891 AD Scoria

General Textural Observations

Thin section - Certain textural features are common throughout most of the Foerstner scoria deposits. Vesicles contained within sideromelane groundmass are typically more abundant but smaller in size, while those found in tachylite are fewer but larger in size. Small vesicles (i.e., L<0.2 mm) are typically round while larger vesicles become increasingly irregular with non-circular outlines. Vesicle walls are smooth, and bubbles are found adjacent to both groundmass and crystals. There is no evidence of shearing as evidenced by the lack of elongated vesicle trains.

Tachylite has a higher content of microlites and a lower vesicularity compared to sideromelane (Figure 17a). This is most likely a result of a slower rate of cooling allowing time for microlite nucleation and growth. The transition from sideromelane

to tachylite groundmass observed in the shell of some Foerstner samples can be explained by a variation of cooling rates, as described by Kueppers et al. (2012) for basaltic balloons from the Azores. Upon discharge into seawater, lava instantly cools at a very high rate (up to 1,259 K/s) forming a thin, oxidized crust that consists of rapidly quenched glass (sideromelane) and large vesicles. This crust provides a thermal boundary layer between the incandescent interior of the scoria bomb and cold seawater. The glass beneath the crust is not in direct contact with the seawater and cools at a much slower rate (~30 K/s). This slower rate allows for an extensive nucleation and growth of microlites, leading to the development of tachylite (Figure 17b).

Hand sample – One scoria balloon collected from the Foerstner vent site was preserved almost intact (Figure 18). The balloon-like structure is 45 cm long and is made up of a thin lava shell surrounding a hollowed interior, corresponding to an abundance of individual remnant vesicles separated by thin walls. The total thickness of the shell is 2-4 cm and it is comprised of two distinct layers (Figure 19). A reddish-brown, oxidized quenched crust covers the exterior of the balloon and is colonized by hard tubeworm and coral casts. This outer layer is very thin and vesicular and does not exceed a maximum thickness of about 2 mm. The dominant portion of the lava crust consists of a dark grey, less vesicular tachylite layer that is beneath the oxidized crust. Vesicles contained within the shell are abundant, but millimetric in size and are elongated along planes parallel to the long axis of the balloon. Larger pore spaces along the exterior of the bomb are commonly filled with pelagic clay. The transition between the lava shell and hollowed interior is marked by a thin (<1 mm), white

horizon that may have been formed by gas condensates. The surface facing the large central cavity is covered in abundant septa, interpreted as the remnants of vesicles walls. The aphanitic groundmass is bluish-gray in color with vesicles up to 5 cm in diameter based on measurements of the remnant walls.

Vesicle Textures

Degassing processes of balloon formation were investigated by determining vesicle size distributions using the methods of Shea et al. (2010). Vesicle volume distribution (VVD) of a scoria balloon bomb (NA018-017) displays a negative skewness with an extended tail towards small vesicles (Figure 20). Vesicles range from 0.01 to 1.585 mm in diameter. The distribution shows a progressive disappearance of smaller vesicles with a dominant mode in vesicle size at 0.63 mm.

The VVD plot of a spatter-like deposit recovered from the summit of the main vent (NA018-021) displays a narrow distribution with low amplitudes and a minor mode at 0.43 mm (Figure 21). Vesicles range from 0.01 to 0.859 mm in diameter. The distribution shows negative skewness with an extended tail towards small vesicles. The distribution shows a near absence of smaller vesicles (L<0.1mm).

The VVD plot of a pillow flow lobe fragment recovered from the northwest mound (NA018-027) displays a negative skewness with an extended tail towards small vesicles (Figure 22). Vesicles range from 0.027 to 1.08 mm in diameter. The distribution shows a progressive disappearance of smaller vesicles with a dominant mode at 0.43 mm.

The VVD plot of a scoria bomb representative of those observed at Foerstner recovered from the large western vent (NA018-032) displays a negative skewness with

an extended tail towards small vesicles (Figure 23). Vesicles range from 0.01 to 1 mm in diameter. The distribution shows a progressive disappearance of smaller vesicles with a major mode between 0.32 and 0.63 mm (ignoring the significant drop off in volume fraction at 0.5 mm).

Interpretations and Discussion

Bubble formation and growth within AD 1891 magmas

A comparison of bubble texture data from samples of AD 1891 deposits allows inferences to be made about magma degassing processes. Samples were chosen to cover the major lithofacies found at the Foerstner vent site and surrounding seafloor. These include scoria balloon bomb (NA018-17), spatter (NA018-21), pillow flow lobe (NA018-27), and scoria bomb bed (NA018-32). In particular, the vesicle volume distribution (VVD) plots can provide useful insights into processes of bubble growth, coalescence, and ripening (Shea et al. 2010).

All four samples exhibit generally unimodal distributions on VVD plots (Figures 20-23) suggesting a single distinct pulse of nucleation and growth (Shea et al. 2010). The negative skewness, also observed on all four plots, is interpreted to be a consequence of bubble ripening during the course of the eruption.

The bubble sizes and spatial distributions observed in the Foerstner samples suggest that growth resulted from the steady diffusive transfer of gas between bubbles through films. This transfer process, known as Ostwald ripening, is driven by the pressure excess inside bubbles, which is high for small bubbles and low for large bubbles (Mangan and Cashman 1996). Since the bubble distribution within magma is

generally polydispersed, internal pressures will be irregular. As bubbles occupy a greater volume of the melt (usually near the vent surface), the nearest-neighbor distance becomes smaller and gas diffuses from regions of high to low pressure. As a result, large bubbles grow and small bubbles shrink or may disappear altogether (Mangan and Cashman 1996). In this respect, the process differs from coalescence, which is driven by mechanical and molecular interactions resulting in a more favorable thermodynamic condition, but is not actually driven by surface energy (Herd and Pinkerton 1997).

The progressive disappearance of small, and enrichment of large vesicles is observed in all VVD plots (Figures 20-23). As in coalescence, the foam coarsens as magma residence time in the conduit increases and the surface area of the gas-melt interface decreases. However, individual bubbles shrink or grow gradually during ripening, and a normal rather than polymodal bubble size frequency distribution evolves (Mangan and Cashman 1996). Studies have shown that ripening has a significant influence in the bubble textures of basaltic fire-fountain eruptions (Mangan and Cashman 1996). Additionally, it has been observed that Strombolian activity at Heimaey, Iceland was controlled by the bursting of large, individual bubbles (Blackburn et al. 1976) such as those that are formed by ripening. Further discrimination between Hawaiian fire fountaining and Strombolian-type eruption mechanisms cannot be deduced from these data.

Facies Distribution and Eruption Model

Eruption mechanisms that vary from dominantly effusive to explosive have been proposed to explain the production of floating scoria and their subsequent

deposition. Gaspar et al. (2003) and Kueppers et al. (2012) proposed that the magma involved in the Serreta submarine ridge eruption was fluid and gas-rich, favoring the segregation and accumulation of gas under a cooler lava crust at vent level. They proposed the development of large gas bubbles within the magma just below the crust. At a critical point of accumulation, these large gas bubbles form blisters that, in a subaqueous setting, detach from the lava surface as swollen lava balloons and rise by flotation. In contrast, Siebe et al. (1995) proposed that intermittent lava fountaining could be responsible for the production of floating scoria bombs, as well as other pyroclastic deposits and pillow flows. Fountaining results from changes in eruption velocities due to variation in exsolved volatile content. While most of the clasts fall out close to the vent, some gas-charged magma could produce highly vesiculated scoria that rise to the surface (Smith and Batiza 1989). At the summit of Foerstner volcano there was no evidence for a solidified lava lake or extensive pillow flow lobes. Thus, the dominant clastic nature of the vent site points more strongly to a dynamic explosive mechanism for balloon formation.

The dominant ripening degassing process determined by analyzing the bubble size distributions of Foerstner deposits favors either a Hawaiian fire fountaining or Strombolian-type eruption mechanism. Each of these eruption types are characterized by fluctuating magma discharge rates due to changing exsolved volatile contents (Siebe et al. 1995; Pioli et al. 2009). Either submarine fire fountaining or Strombolian activity could explain the deposition of abundant pyroclastic deposits as well as the effusive lava flow deposits observed at the main vent site. Magma eruption velocities are unlikely to remain constant for extended periods of time; instead they would

fluctuate as observed at subaerial lava fountains (Head and Wilson 1987). Periods of rapid gas exsolution would promote explosive eruptions and their subsequent deposits, while waning exsolution promotes effusive eruptions (Pioli et al 2009).

The diversity of facies observed at the Foerstner vent site are most likely a result of varying magma rise speed in the feeding conduit, enhanced volatile content of the source alkali basalt, and generally low viscosity of the magma. These factors promote differential rise speeds of melt and bubbles allowing large, early-nucleated bubbles to migrate upward in the conduit as a slug flow and overtake smaller, later-nucleated bubbles. The emergence of these large bubbles through magma within the conduit drives Strombolian type eruptions (Head and Wilson 2003). This erupted magma would have contained a lower fraction of small vesicles as they were overtaken by larger, more energetically stable bubbles. The lack of small gas bubbles limits the disruption of erupted lava into smaller fragments, allowing for very large magma clots to be ejected at sizes comparable to the width of the conduit (Head and Wilson 2003). This mechanism could explain the deposition of scoria bombs up to 2 meters in size observed on the flanks of Foerstner.

Head and Wilson (2003) made predictions about the resulting deposits and landforms of submarine Strombolian eruptions. The initial stages of a Strombolian eruption are characterized by dike emplacement and extrusion of lavas at very low discharge rates. This leads to the deposition of short flows and pillows rather than extensive lobate sheets (Head et al. 1996; Gregg and Fink 1995), much like the well-defined pillow flow lobes forming linear ridges that emanate radially towards the northwest and west from the main Foerstner vent (Figure 10). As magma rise rates

increase and stabilize, typical Strombolian activity occurs as the gas bubble rise rate exceed that of the magma. Explosive disruption of the magma occurs at the vent-water interface, producing fragmental deposits that typically fall within 10-20 m from the vent as a result of hydrodynamic drag and subsequent deceleration of pyroclastic fragments. The larger blocks and bombs (64 to >256 mm in diameter) that constitute the major facies observed at Foerstner most likely formed from the plug of magma ejected in front of the larger rising gas bubbles. Smaller fragments quickly settle near the vent upon ejection as a result of their low inertia and accumulate as agglutinate. Deposits of this kind may correspond to spatter-like deposits observed at the summit of Foerstner.

In general, explosive Strombolian activity becomes localized at the cone vent, while lava flows emerge from lateral vents located at the base of the cone (Valentine et al. 2005; Pioli et al. 2009). This type of vent morphology is observed at Foerstner as the main vent site is dominated by explosive pyroclastic deposits and the three smaller mounds observed immediately to the northwest are constructed of pillow flow lobes. Simultaneous eruption of pyroclastics from the cone and lava flows from the lateral vents requires segregation of a low viscosity, exsolved volatile-rich magma into a gas-rich mixture that ascends through the central conduit and gas-poor lava flowing laterally. Observations of Strombolian activity at Paricutin volcano in Mexico showed that the mass eruption rate (MER) controlled the proportion of magma emitted by explosive vs. effusive activity and the initial formation of lateral vents increased the explosivity of eruptions occurring at the cone (Pioli et al. 2009). Dual activity of this type requires a MER of 10^3 to 10^5 kg/s and when this drops to a rate below 10^3 kg/s,

degassing dominates producing either lava effusion or mild explosive activity (Pioli et al. 2009).

The pyroclastic deposits that occur on Foerstner can be distinguished from submarine fire fountain eruption products by the dominance of large scoriaceous clasts deposited near the vent, a spatter-like vent facies, lack of extensive pyroclastic flow deposits, and short, pillow textured flows. If Hawaiian-style fountaining was the dominant eruption mechanism, the predicted deposits would include vesicular sheet flows, partly agglutinated distal fragments, relatively small grain sizes, and abundant pyroclastic flows surrounding the cone (Head and Wilson 2003).

Thus, we propose that Strombolian activity was the most likely eruption style displayed by the Foerstner 1891 eruption on the basis of the high proportion and sizes of pyroclastic deposits and the presence of clastic-dominated vent cones with smaller laterally distributed vents with effusive products (pillow flow lobes). Similar interpretations were reached by Clague et al. (2002) about eruptive products recovered along the Kilauea rift zone and Gorda Ridge axis. From alkali basalt vents on the south side of Kaua'i, Clague et al. (2002) described highly vesicular spatter, breadcrust bombs, and agglutinated spatter as representative of Strombolian-style eruptions.

Although we use the term Strombolian style to describe the eruption mechanism it is noted that there are fundamental differences between the behaviors of Strombolian events in the subaerial versus the submarine environment. First, the presence of water significantly dampens the dispersal of fragmented clasts in the submarine environment and will likely affect the resulting morphology at the vent

area. In the subaerial environment Strombolian activity produces scoria cones with a central crater because fragmented clasts are able to be dispersed over relatively large distances (>100 m) by ballistic trajectories through the atmosphere. Underwater, the drag effect restricts dispersal and likely builds a mound-like cone without a well-defined central crater. Second, in the submarine environment gas-rich magma can attain positive buoyancy relative to seawater prior to fragmentation (Friedman et al. 2012; Rotella et al. 2013). This condition, which can never be attained in the subaerial environment, can dramatically affect the nature of submarine eruptions. Positive buoyancy flux results in a potentially complex globular discharge of highly vesicular magma that then fragment by gas expansion (Friedman et al. 2012). This style of activity was captured by ROV photography on West Mata submarine volcano in the Pacific (Rubin et al. 2012, fig. 2b).

Assuming that Foerstner exhibited Strombolian-type eruptive activity, predictions can be made about the generation of the lava balloons. We suggest that discharge of magma at the vent-seawater interface produced batches of coarse magma "blobs" that rapidly cooled and decelerated upon contact with the surrounding seawater. Since magma erupted from Strombolian activity is typically a gas-rich froth rather than liquid, many of these blobs have the potential to be extremely vesicular and thus buoyant relative to seawater. Maximum bubble sizes for submarine Strombolian eruptions can reach up to 1.5-2 m in size as a result of higher ambient pressure (Head and Wilson 2003). Data from other studies suggest that the exterior of these fragments can hyperquench with a cooling rate of ~1,259 K/s to form a solid lava shell that acts as an insulating layer preventing the magmatic gas in its interior from escaping

(Kueppers et al. 2012). These extremely vesicular bombs attained densities less than 1000 kg/m^3 and thus can rise buoyantly to the surface. Magma forming these rising balloons continued to degas as the ambient pressure decreases leading to balloon inflation. This expansion leads to enlargement of the balloons' surface area and formation of new skin. This process is facilitated by the presence of still-molten lava inside the balloon, which prevents complete rupture of the outer solid crust. Some lava balloons collected off the sea surface in 1891 were noted to still have molten, red-hot interiors (Butler 1892).

All other known occurrences of floating scoria have been associated with a relatively narrow water depth range between 30 and 1000 m (Siebe et al. 1995; Kueppers et al. 2012; Rivera et al. 2013), but with the best-defined source vents being located within a more limited range of only 200 to 400 m. It is likely that at depths greater than 400 m, confining pressures prevent the degree of volatile exsolution required to generate extremely vesicular magma that is buoyant relative to seawater. In contrast, at depths shallower than 200m, extremely low pressures promotes rapid volatile exsolution and a high degree of fragmentation preventing the discharge of coarse magma blobs. At such shallow depths highly explosive activity is likely driven by phreatomagmatic explosions in addition to primary degassing (Sigurdsson et al. 1999). The presence of highly inflated scoria bombs in association with a dominantly clastic vent site, as observed at Foerstner, may represent a paleoenvironmental indicator for modern and ancient basaltic shallow submarine eruptions at depths of several hundred meters.

Conclusions

Scoria balloons observed floating on the sea surface 4 km west of the town of Pantelleria at the northwest end of the island were the product of a submarine eruption at Foerstner volcano in 1891 AD. The subspherical balloons are made up of a thin sideromelane/tachylite lava shell a few cm in thickness surrounding a hollowed interior and have a tephrite basanite composition. Vesicle size distributions of four Foerstner samples show a progressive disappearance of small vesicles (L<0.1 mm) and increased abundance of larger vesicles as a result of Ostwald ripening, a common degassing process that drives Hawaiian fire fountaining and Strombolian type eruptions. ROV exploration of the Foerstner vent site revealed a variety of explosive and effusive type deposits and small lateral mounds made up of pillow flow lobes. The main Foerstner vent is constructed of two overlapping circular mounds with a total volume of 6.28×10^5 m^3 and relief of 60 m.

Based on the facies observed at Foerstner and the inferred degassing processes, a model was developed for an eruption style that produces floating scoria balloons during the 1891 submarine eruption. A likely mechanism for the formation of buoyant scoria is Strombolian style eruptions occurring over a shallow depth range between 200 and 400 m, as water depth (hydrostatic pressure) is the primary control on the vesicularity of erupted basalt. The initial stages of the 1891 AD Foerstner eruption consisted of dike emplacement and extrusion of lava at very low discharge rates, producing short, pillow flow lobes that emanate from the center of the vent to the northwest and west. Typical Strombolian activity soon followed as the gas bubble rise rate exceeded that of the magma. Explosive disruption of the magma occurred at the

vent-water interface and produced coarse fragmental deposits that fell on the slopes, while smaller fragments quickly settled near the vent and accumulated as spatter-like deposits. We suggest that buoyant scoria bombs were formed from the rapid cooling of extremely vesicular magma blobs. The exterior of these fragments hyperquenched forming a solid lava shell that acted as an insulating layer preventing magmatic gas in its interior from escaping. The bombs attained densities less than 1000 kg/m^3 and thus rose buoyantly to the surface. Rupture of the outer solid crust was prevented by the presence of a still-molten interior that accommodates expansion by progressive thin crust formation.

Lava balloon eruptions may occur more frequently than previously thought. The eruptive conditions that characterize these products are now better documented and likely occur in a variety of submarine volcanic environments: low silica alkalic magma (43-52% SiO_2), high volatile content (CO_2, H_2O), and low hydrostatic pressures (water depths between ~200-400 m). Most historical balloon eruptions had durations of days to weeks, providing a very small window of time to allow for their detection by direct observation, seismology, or remote sensing. Only the Serretta Ridge eruption in the Azores lasted for a year or longer (Gaspar et al. 2003; Kueppers et al. 2012). Identifying and monitoring active submarine volcanoes that satisfy the eruptive conditions described above could lead to further *in situ* studies of balloon producing eruptions. Finally, we envision that the facies relationships documented at the Foerstner vent site can be used as a paleoenvironmental model for ancient basaltic shallow (200-400 m) submarine eruptions.

References

Argnani A (1990) The Strait of Sicily Rift Zone: foreland deformation related to the evolution of a back-arc basin. J Geodyn 12:311–331

Beccaluva L, Colantoni P, DiGirolamo P, Savelli C (1981) Upper-Miocene Submarine Volcanism in the Strait of Sicily (Banco senza Nome). Bull Volcanol 44(3)573-581

Blackburn EA, Wilson L, Sparks RSJ (1976) Mechanisms and dynamics of strombolian activity. J Geol Soc Lond 132:429-440

Bosman A, Calarco M, Casalbore D, Chiocci FL, Coltelli M, Conte AM, Martorelli E, Romagnoli C, Sposato A (2007) New insights into the recent submarine volcanism of Pantelleria Island. Gruppo Nazionale di Geofisica della Terra Solida abstract session 1.3: 177-178

Burollet PF, Mugniot JM, Sweeney P (1978) The geology of the Pelagian block: the margins and basins of southern Tunisia and Tripolitania. In: Nairn, A.E.M., Kanes, W.H., Stelhi, F.G. (Eds.), The Ocean Basins and Margins. The Western Mediterranean 4b:331–359

Butler GW (1892) Abstract of Mr A Ricco's account of the submarine eruption northwest of Pantelleria, October 1891. Nature 45:584-585

Calanchi N, Colantoni P, Rossi PL, Saitta M, Serri G (1989) The Strait of Sicily continental rift system: Physiography and petrochemistry of the submarine volcanic centres. Mar Geol 87:55-83

Cello G, Crisci GM, Marabini S, Tortorici L (1985) Transtensive tectonics in the strait

of Sicily: structural and volcanological evidence from the island of Pantelleria. Tectonics 4(3):311–322

Civetta L, Cornette Y, Gillot PY, Orsi G (1988) The eruptive history of Pantelleria (Sicily Channel) in the last 50 ka. Bull Volcanol 50:47-57

Civetta L, Cornette Y, Crisci G, Gillot PY, Orsi G, Requejos CS (1984) Geology, geochronology, and chemical evolution of the Island of Pantelleria. Geol Mag 121: 541-668

Civile D, Lodolo E, Accettella D, Geletti R, Ben-Avraham Z, Deponte M, Facchin L, Ramella R, Romeo R (2010) The Pantelleria graben (Sicily Channel, Central Mediterranean): an example of intraplate 'passive' rift. Tectonophysics 490:173–183

Civile D, Lodolo E, Tortorici L, Lanzafame G, Brancolini G (2008). Relationships between magmatism and tectonics in a continental rift: The Pantelleria Island region (Sicily Channel, Italy). Mar Geol 251(1-2):32-46

Clague DA, Davis AS, Dixon JE (2002c) Submarine strombolian eruptions in Hawaii and along the Gorda Mid-ocean Ridge. In: Explosive Subaqueous Volcanism. Am Geophysical Monograph, American Geophysical Union, Washington, DC

Corti G, Cuffaro M, Doglioni C, Innocenti F, Manetti P (2006) Coexisting geodynamic processes in the Sicily Channel. Geol Soc Am 409:83–96 Special paper

Cox KG, Bell JD, Pankhurst RJ (1979) The Interpretation of Igneous Rocks. George Allen & Unwin, London

Friedman PD, Carey S, Raessi M (2012) Influence of volatile degassing on initial flow structure and entrainment during undersea volcanic fire fountaining eruptions. Nat Sci 4(12):1-11

Gaspar JL, Queiroz G, Pacheco JM, Ferreira T, Wallenstein N, Almeida MH, Coutinho R (2003) Basaltic Lava Balloons Produced During the 1998-2001 Serreta Submarine Ridge Eruption (Azores), in Explosive Subaqueous Volcanism, edited by White, J., Clauge, D., and Smellie, *J Am Geophys Un* 140:205-212

Gregg TKP, Fink JH (1995) Quantification of submarine lava-flow morphology through analog experiments. Geology 23:73-76

Head JW, Wilson L (1987) Lava fountain heights at Pu'u 'O'o, Kilauea, Hawai'i: indicators of amount and variations of exsolved magma volatiles. J Geophys Res 92:13715-13719

Head JW, Wilson L (2003) Deep submarine pyoclastic eruptions: theory and predicted landforms and deposits. J Volcanol Geotherm Res 121:155-193

Head JW, Wilson L, Smith DK (1996) Mid-ocean ridge eruptive vent morphology and structure: Evidence for dike widths, eruption rates, and evolution of eruptions and axial volcanic ridges. J Geophys Res 101:28265-28280

Herd RA, Pinkerton H (1997) Bubble coalescence in basaltic lava: its impact on the evolution of bubble populations. J Vol Geotherm Res 75:137-157

Houghton BF, Wilson CJN (1989) A vesicularity index for pyroclastic deposits. Bull Volcanol 51:451-462

Illies, JH (1981) Graben formation: The Maltese Island—A case history.

Tectonophysics, 73:151–168

Kelley KA, Plank T, Ludden J, Staudigel H (2003) Composition of altered oceanic crust at ODP Sites 801 and 1149. Geochem Geophys Geosyst 4(6):8910

Kueppers U, Nichols ARL, Zanon V, Potuzak M, Pacheco JMR (2012) Lava balloons – peculiar products of basaltic submarine eruptions. Bull Volcanol 74:1379-1393

Mangan MT, Cashman KV (1996) The structure of basaltic scoria and reticulite and inferences for vesiculation, foam formation, and fragmentation in lava fountains. J Volcanol Geotherm Res 73:1-18

Martorelli E, Petroni G, Chiocci FL, Bosman A, Calarco M, Conte AM, Macelloni L, Salusti E, Sposato A (2011) Contourites offshore Pantelleria Island (Sicily Channel, Mediterranean Sea): depositional, erosional and biogenic elements. Geo-Marine Letters 31:481–493

Moore JG, Fornari DJ, Clague DA (1985) Basalts from the 1877 submarine eruption of Mauna Loa, Hawaii: New data on the variation of the palagonization rate with temperature. US Geol Surv Bull 1663

Morris RV, Gooding JL, Lauer HV, Singer RB (1990) Origins of Marslike spectral and magnetic properties of a Hawaiian palagonitic soil. J Geophys Res 95:14,427-14,434

Morrisey M, Zimanowski B, Wohletz K, Buettner R (1999) Phreatomagmatic fragmentation. In: Sigurdsson H (ed) Encyclopedia of Volcanoes, 1st edn. Academic Press, New York, pp 431-445

Pearce JA (1983) Role of the sub-continental lithosphere in magma genesis at active continental margins. In Continental Basalts and Mantle Xenoliths, ed. CJ

Hawkesworth, MJ Norry, pp. 230-49. Nantwich, UK: Shiva

Pearce JA, Norry MJ (1979) Petrogenetic implications of Ti, Zr, Y, and Nb variations in volcanic rocks. Contrib Mineral Petrol 69:33-47

Peccerillo A (2005) Plio-Quaternary volcanism in Italy: Petrology, Geochemistry, Geodynamics. Springer, Heidelberg

Pioli L, Azzopardi BJ, Cashman KV (2009) Controls on the explosivity of scoria cone eruptions: Magma segregation at conduit junctions. J Volcanol Geotherm Res 186:407-415

Rivera J, Lastras G, Canals M, Acosta J, Arrese B, Hermida N, Micallef A, Tello O, Amblas D (2013) Construction of an oceanic island: Insights from the El Hierro (Canary Islands) 2011-2012 submarine volcanic eruption. Geology 41(3):355-358

Rotolo SG, Castorina F, Cellula D, Pompilio M (2006) Petrology and geochemistry of submarine volcanism in the Sicily channel. J Geol 114:355-365

Rotella MD, Wilson CJN, Barker SJ, Wright IC (2013) Highly vesicular pumice generated by buoyant detachment of magma in subaqueous volcanism. Nature doi:10.1038/NGEO1709

Rubin KH, Soule SA, Chadwick Jr WW, Fornari DJ, Clague DA, Embley RW, Baker ET, Perfit MR, Caress DW, Dziak RP (2012) Volcanic eruptions in the deep sea. Oceanography 25(1):142-157, http://dx.doi.org/10.5670/oceanog.2012.12

Shea T, Houghton BF, Gurioli L, Cashman KV, Hammer JE, Hobden BJ (2010) Textural studies of vesicles in volcanic rocks: An integrated methodology. J Volc Geotherm Res 190:271-289

Siebe C, Komorowski JC, Navarro C, McHone J, Delgado H, Cortes A (1995) Submarine eruption near Socorro Island, Mexico: Geochemistry and scanning electron microscopy studies of floating scoria and reticulite. J Volc Geotherm Res 68(4):239-271

Simpson K, McPhie J (2001) Fluidal-clast breccia generated by submarine fire fountaining, Trooper Creek Formation, Queensland, Australia. J Volc Geotherm Res 109:339-355

Smith TL, Batiza R (1989) New field and laboratory evidence for the origin of hyaloclastite flows on seamount summits. Bull Volcanol 51:96–114

Taddeucci J, Pompilio M, Scarlato P (2004) Conduit processes during the July-August 2001 explosive activity of Mt. Etna (Italy): inferences from glass chemistry and crystal size distribution of ash particles. J Volcanol Geotherm Res 137:1-3, 33-54

Troll VR et al. (2012) Floating sandstones off El Hierro (Canary Islands, Spain): the peculiar case of the October 2011 eruption. Solid Earth Dis 3:975–999

Valentine G, Krier D, Perry FV, Heiken G (2005) Scoria cone construction mechanisms, Lathrop wells volcano, southern Nevada, USA. Geology 33:629-63

Washington HS (1909) The submarine eruptions of 1831 and 1891 near Pantelleria. Am J Sci 27: 131-150

Table 1. Description of samples from Foerstner submarine volcano

Sample[1]	Latitude[2]	Longitude	Depth (m)	ROV Dive	Description
NA018-017	36º 50.8669' N	11º 53.2302' E	350	H1205	Scoria balloon bomb, oxidized
NA018-018	36º 50.8675' N	11º 53.2157' E	348	H1205	Whole scoria balloon bomb
NA018-019	36º 50.6993' N	11º 53.4700' E	253	H1205	Scoria bomb, moderately vesicular
NA018-020	36º 50.6875' N	11º 53.4714' E	259	H1206	Scoria bomb, heavy sedimentation/encrustations, oxidized
NA018-021	36º 50.6847' N	11º 53.4800' E	249	H1206	Spatter, dense, poorly vesicular
NA018-022	36º 50.6784' N	11º 53.4765 E	252	H1206	Scoria bomb, highly vesicular, oxidized
NA018-023	36º 50.6485' N	11º 53.4781' E	288	H1206	Scoria bomb, highly vesicular, heavily oxidized/sedimented
NA018-024	36º 50.6451' N	11º 53.4798' E	294	H1206	Scoria bomb, highly vesicular, abundant encrustations, heavily oxidized/sedimented
NA018-025	36º 50.5598' N	11º 53.4814' E	308	H1206	Scoria flow lobe fragment, heavily encrusted
NA018-026	36º 50.6314' N	11º 53.4568' E	320	H1206	Vesciulated scoria, oxidized, long internal vesicles
NA018-027	36º 50.2708' N	11º 53.4039' E	343	H1206	Pillow flow lobe fragment, oxidized, encrusted, sedimented
NA018-029	36º 50.7646' N	11º 53.4057' E	346	H1207	Pillow flow lobe fragment, glassy quench crust
NA018-030	36º 50.7646' N	11º 53.4057' E	346	H1207	Pillow flow lobe fragment, dense, oxidized crust, large internal vesicles
NA018-031	36º 50.7536' N	11º 53.2993' E	338	H1207	Pillow flow lobe fragment, black, encrustations
NA018-032	36º 50.6938' N	11º 53.0622' E	201	H1207	Scoria bomb, highly vesicular, heavily oxidized/sedimented
NA018-033	36º 50.6797' N	11º 53.0000' E	223	H1207	Scoria bomb, highly vesicular, oxidized

[1]NA018 - *E/V Nautilus* cruise in 2011

[2]Latitude and longitude from raw ROV navigation data

Table 2. Major element XRF bulk compositional analyses of representative *in situ* scoria samples from Foerstner submarine volcano

Sample	NA018-019	NA018-021	NA018-022	NA018-023	NA018-025	NA018-026	NA018-027	NA018-030	NA018-032	NA018-033
Major elements (wt%)										
SiO_2	44.7	44.6	44.7	44.2	47.0	44.7	44.9	44.7	43.9	44.6
TiO_2	4.32	4.30	4.31	4.34	2.57	4.28	4.26	4.22	4.38	4.26
Al_2O_3	13.8	13.6	13.8	14.1	15.9	13.9	13.7	13.5	13.8	13.6
Fe_2O_3	15.5	15.5	15.5	15.6	11.1	15.3	15.3	15.2	15.8	15.4
MnO	0.25	0.24	0.25	0.24	0.17	0.24	0.25	0.24	0.25	0.25
MgO	5.37	5.41	5.42	5.55	6.58	5.23	5.24	5.22	5.78	5.34
CaO	9.82	9.85	9.73	9.60	12.2	9.75	9.85	9.82	9.57	9.99
Na_2O	3.37	3.36	3.44	3.43	2.84	3.28	3.45	3.47	3.48	3.37
K_2O	1.13	1.11	1.13	1.12	0.83	1.14	1.15	1.13	1.08	1.16
P_2O_5	1.77	1.78	1.75	1.73	0.52	1.77	1.78	1.79	1.71	1.75
Total	100	99.75	99.94	99.76	99.71	99.65	99.81	99.4	99.68	99.68
LOI (%)	-0.18	-0.37	0.04	0.55	0.79	-0.34	-0.56	-0.39	1.35	0.43

Table 3. Rare earth element ICP-MS bulk compositional analyses of representative *in situ* scoria samples from Foerstner submarine volcano

Sample	NA018-019	NA018-021	NA018-022	NA018-023	NA018-025	NA018-026	NA018-027	NA018-030	NA018-032	NA018-033
Rare earth elements (ppm)										
La	40.0	40.1	37.9	39.7	22.4	41.2	41.1	38.8	38.8	42.0
Ce	86.0	86.3	80.8	84.2	44.9	87.7	87.1	83.3	83.9	84.5
Pr	11.7	11.7	10.9	11.4	5.74	11.8	11.7	11.5	11.4	11.6
Nd	52.1	52.0	48.3	50.8	24.6	52.1	52.0	50.8	50.9	50.8
Sm	11.1	11.2	10.3	10.9	5.51	11.1	11.1	11.0	11.0	10.7
Eu	4.17	4.14	3.86	4.07	1.93	4.19	4.17	4.10	4.11	4.08
Tb	1.53	1.51	1.42	1.48	0.82	1.53	1.52	1.49	1.51	1.49
Gd	11.2	11.2	10.4	10.9	5.64	11.2	11.1	11.1	11.1	10.9
Dy	8.02	7.89	7.36	7.79	4.46	7.97	7.97	7.81	7.81	7.78
Ho	1.49	1.47	1.36	1.43	0.83	1.47	1.48	1.43	1.44	1.46
Er	3.59	3.53	3.26	3.45	2.04	3.54	3.53	3.43	3.45	3.46
Tm	0.33	0.32	0.30	0.32	0.20	0.33	0.33	0.33	0.33	0.47
Yb	2.74	2.70	2.53	2.68	1.67	2.73	2.73	2.68	2.71	2.73
Lu	0.41	0.40	0.38	0.40	0.25	0.40	0.41	0.40	0.40	0.40

Table 4. Trace element XRF bulk compositional analyses of representative *in situ* scoria samples from Foerstner submarine volcano

Sample	NA018-019	NA018-021	NA018-022	NA018-023	NA018-025	NA018-026	NA018-027	NA018-030	NA018-032	NA018-033
Trace elements (ppm)										
Nb	47	46	47	47	35	47	47	47	47	47
Zr	197	195	196	197	147	196	198	196	198	199
Y	37	37	37	37	21	37	37	36	37	37
Sr	482	481	494	498	529	484	478	480	491	483
U	0	0	0	0	0	0	0	0	0	0
Rb	18	18	19	18	15	18	18	19	18	18
Th	3	3	3	3	2	3	3	3	2	3
Pb	2	2	2	1	3	2	2	2	3	2
Ga	20	20	19	19	18	20	20	19	18	19
Zn	131	125	126	127	99	125	130	126	127	132
Ni	21	21	21	24	83	26	19	18	19	19
Cr	19	16	14	14	217	13	9	10	11	9
V	298	289	276	278	233	278	288	280	266	284
Ce	91	87	89	90	46	87	88	86	88	93
Ba	509	498	498	479	248	504	506	503	439	509

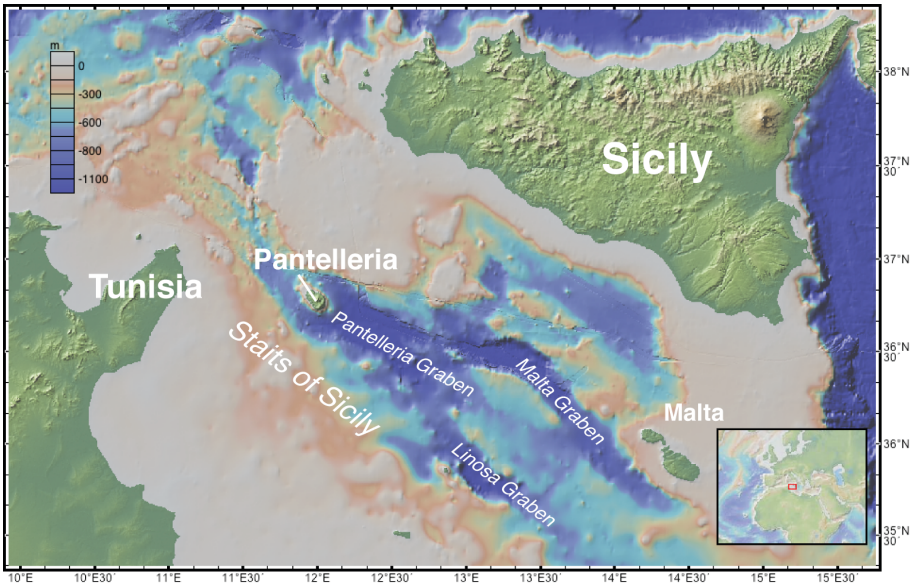

Fig. 1 Bathymetric map of the Straits of Sicily showing locations of volcanic islands and major tectonic features. Inset map shows general location of study area.

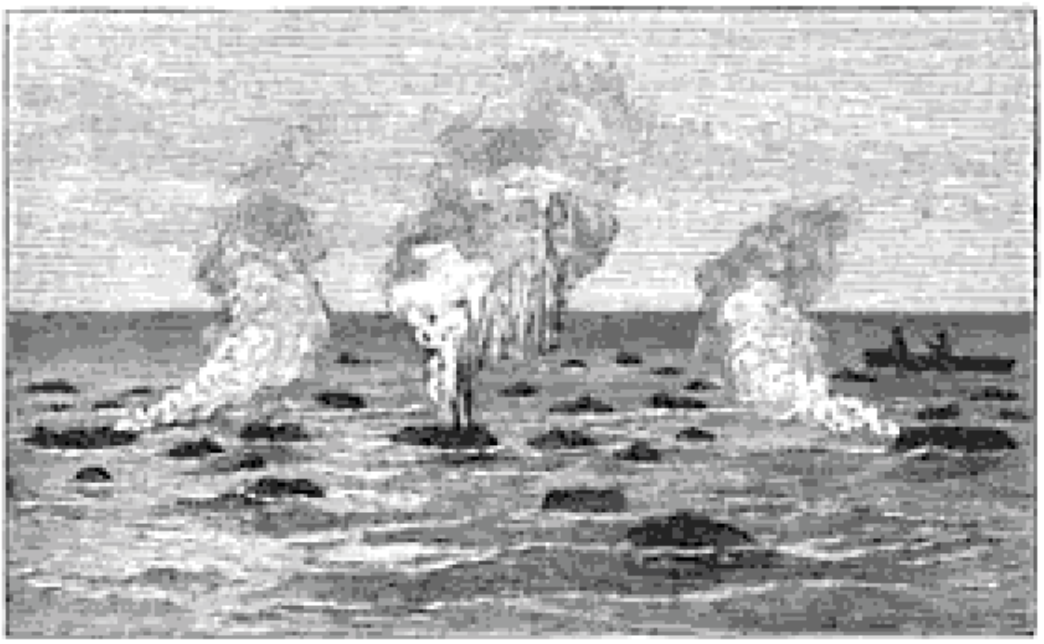

Fig. 2 Lithograph of floating scoria bombs from the 1891 eruption of Foerstner volcano (Butler 1892).

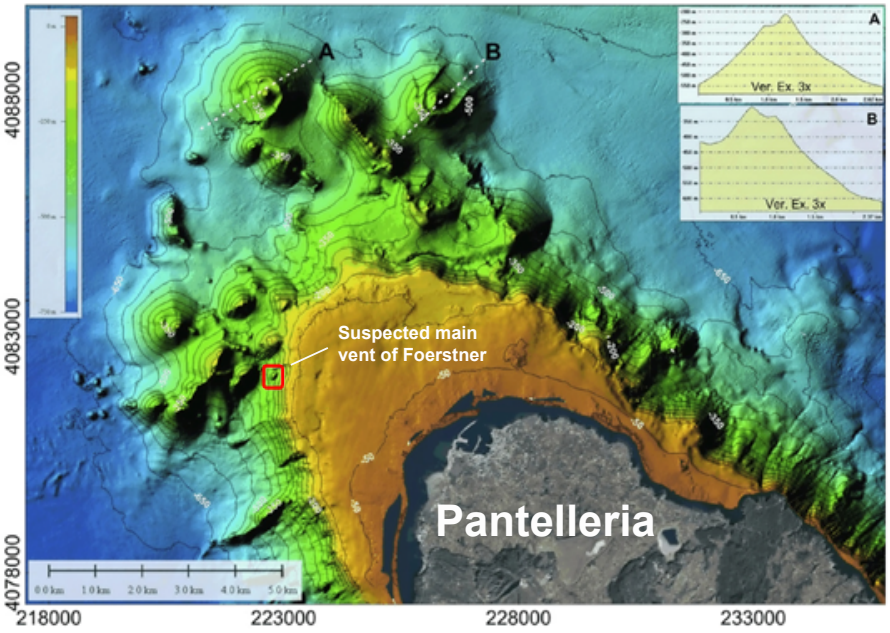

Fig. 3 High resolution bathymetric map showing the suspected location of Foerstner submarine volcano, 4 kilometers northwest of Pantelleria, Sicily (modified from Bosman et al., 2011).

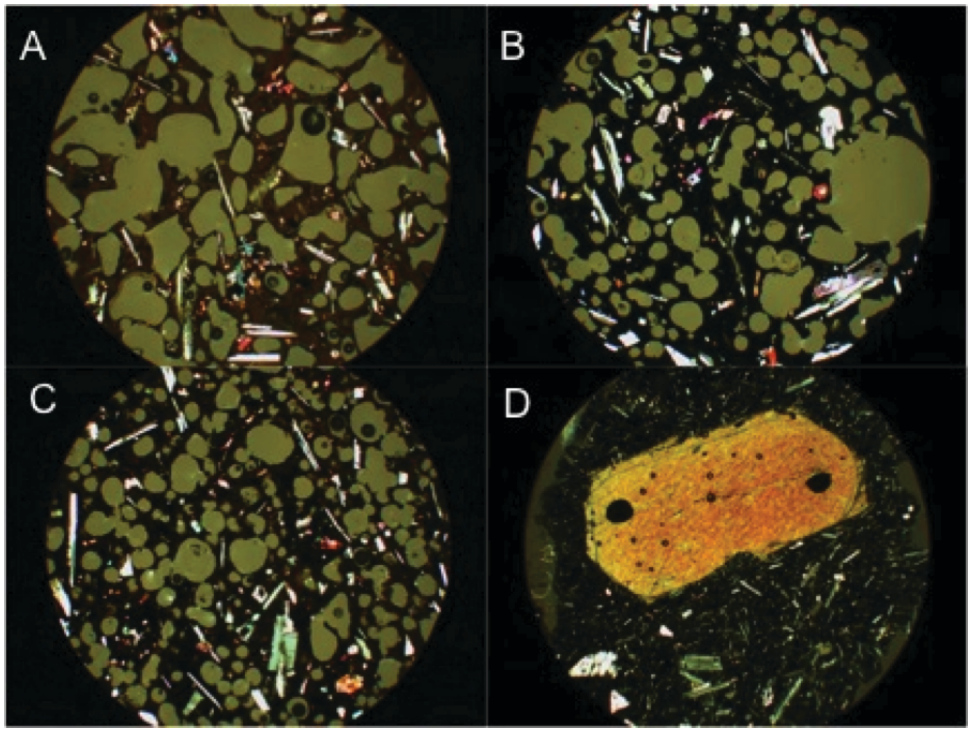

Fig. 4 Overview of groundmass features observed in samples from the 1891 Foerstner eruption. **a** Sample NA018-020 displaying honey-colored sideromelane groundmass and coalesced vesicles. **b** Sample NA018-021 displaying opaque tachylite groundmass. **c** Sample NA018-022 displaying a groundmass consisting of a mixture of tachylite and sideromelane. **d** Sample NA018-025 displaying plagioclase micritic groundmass and a large clinopyroxene phenocryst. The field of view shown is 4 mm in diameter.

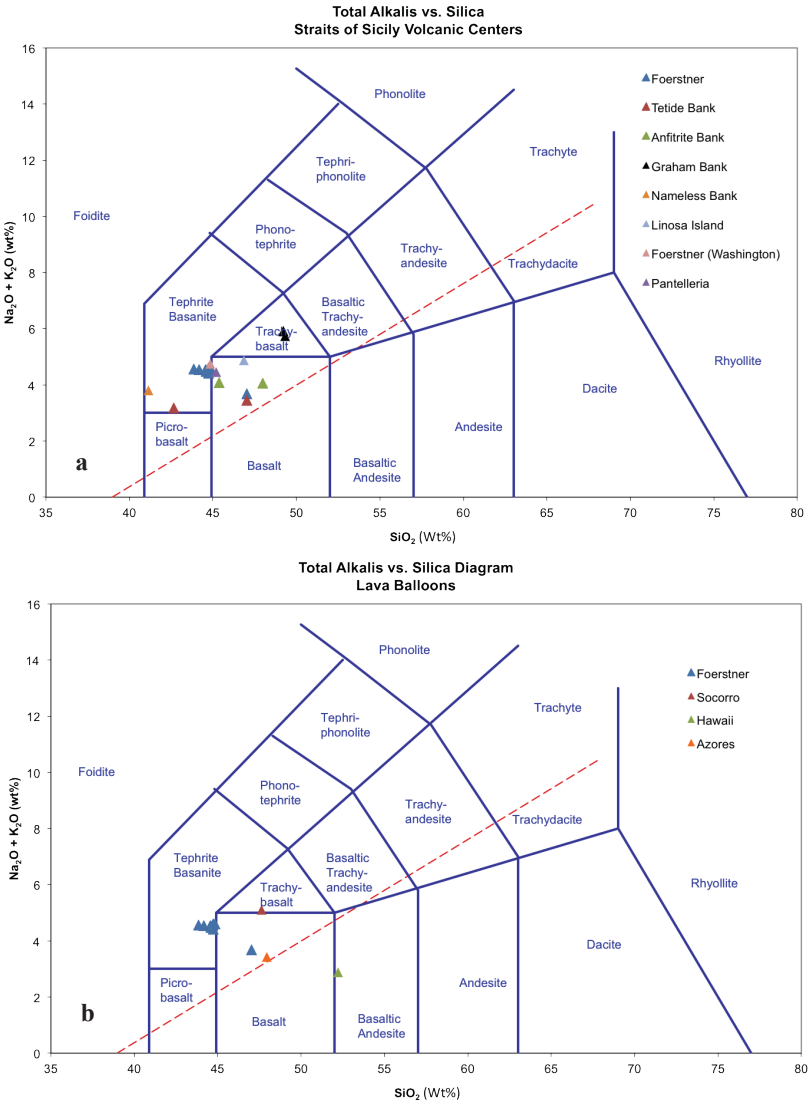

Fig. 5a Average composition of Foerstner basanitic scoria in comparison with samples from other major volcanic centers in the Straits of Sicily as plotted in the TAS diagram after the International Union of Geological Sciences (Calanchi et al., 1988; Washington, 1909; Beccaluva et al., 1981). **b** Average composition of Foerstner basanitic scoria balloons in comparison with all other known submarine lava balloon deposits (Siebe et al., 1995; Moore et al., 1985; Kueppers et al., 2012). Red dashed line discriminates between alkaline and sub-alkaline rocks.

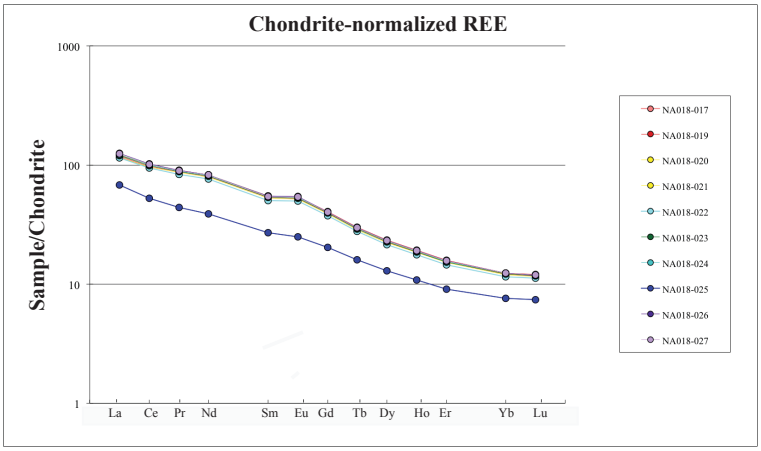

Fig. 6 Chondrite-normalized rare-earth-element composition of Foerstner basanitic scoria (after Nakamura 1974). Significant enrichment (100x) relative to chrondites indicates an oceanic island or continental rift source.

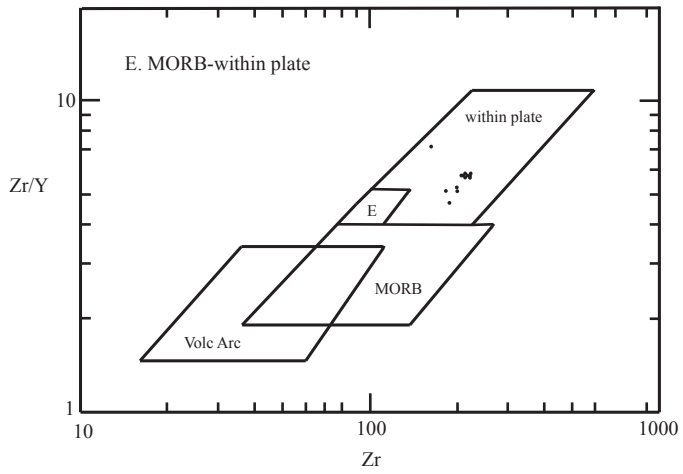

Fig. 7 Distribution of Foerstner basanites on a Zr/Y - Zr tectonic discrimination diagram showing all samples originate from an oceanic island volcanic province (after Pearce and Norry, 1979)

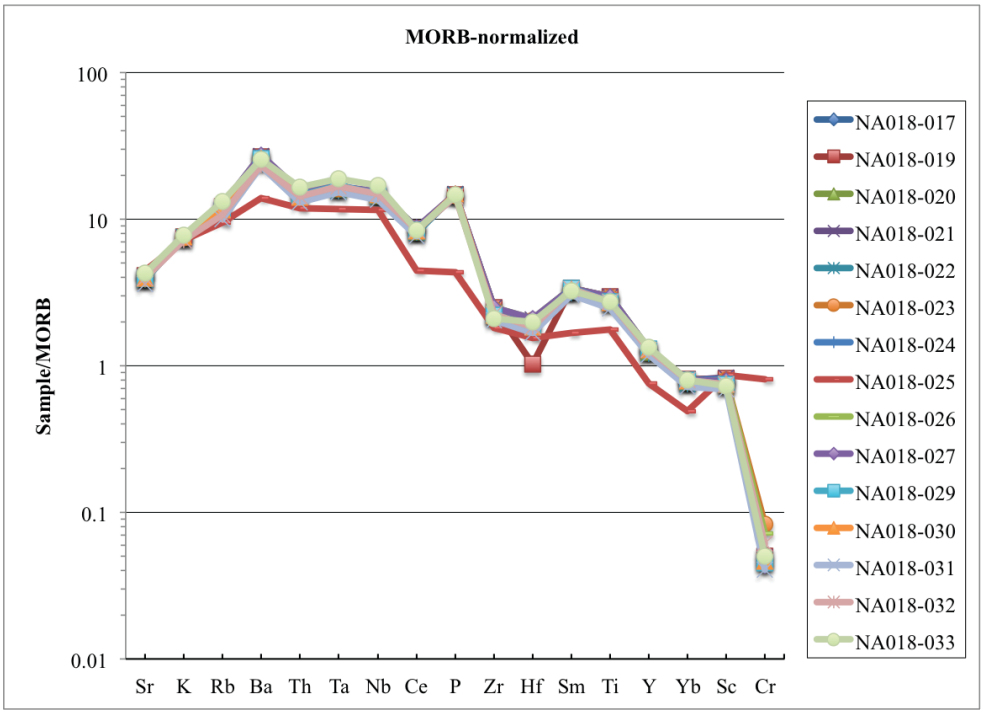

Fig. 8 MORB-normalized trace-element composition of Foerstner basanitic scoria following the procedure of Pearce (1983). Sample NA018-025 shows significant less trace element enrichment relative to the rest of the Foerstner samples indicating it likely originated from a different magma source.

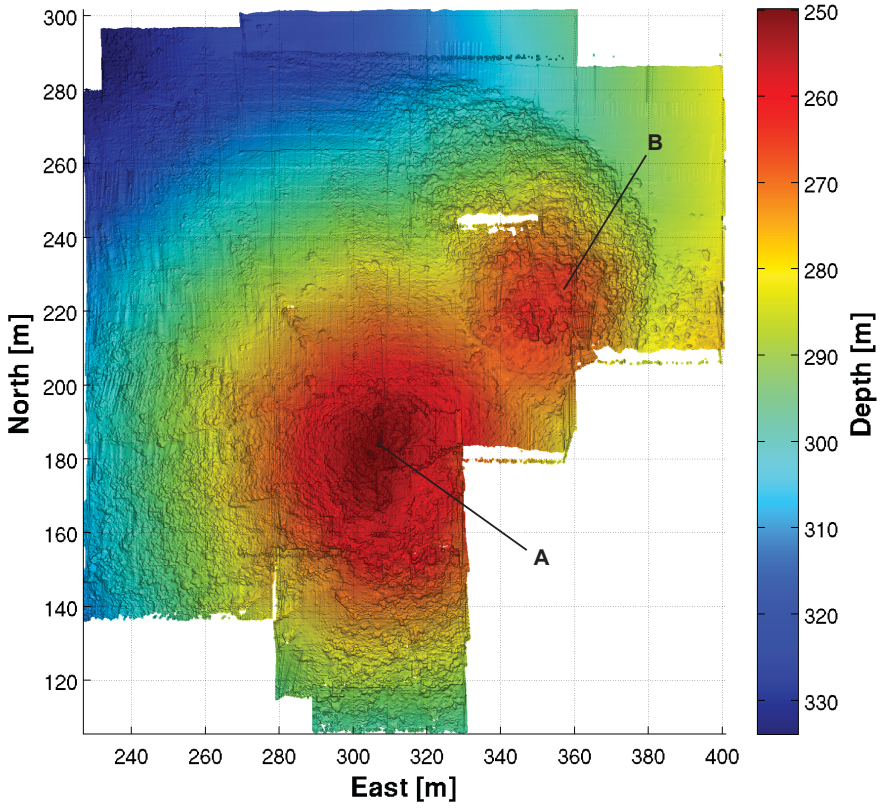

Fig. 9 High-resolution bathymetric map of the suspected Foerstner vent site defining the two peaks (A, B) aligned in a NW-SE direction separated by a narrow saddle region. Latitude and longitude are expressed in local meters.

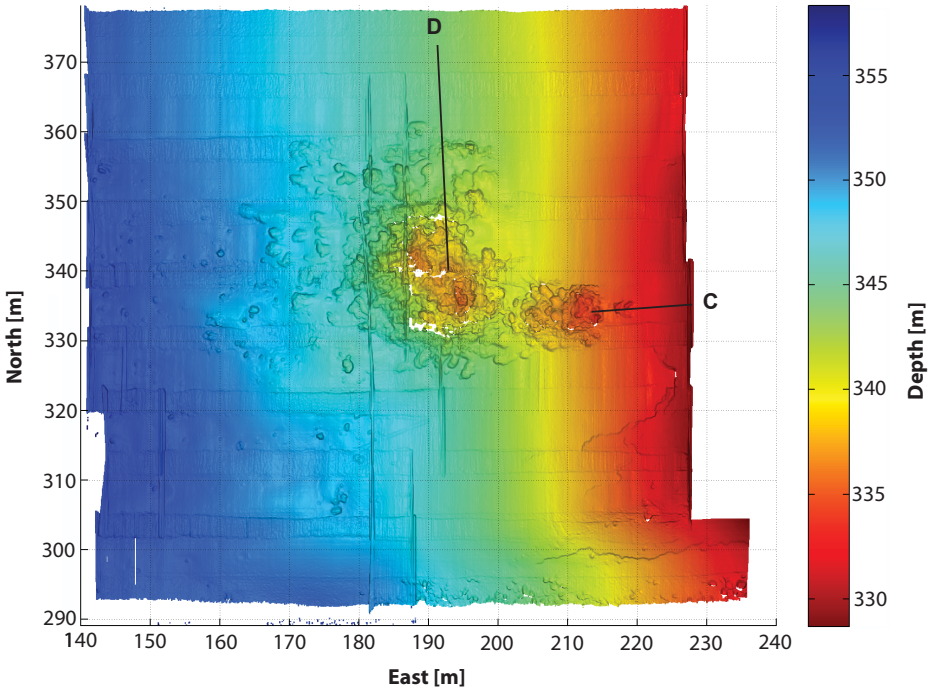

Fig. 10 High-resolution bathymetric map of the small vent area with two peaks (C, D) located 100 meters to the northwest of the suspected main vent of Foerstner. Latitude and longitude are expressed in local meters.

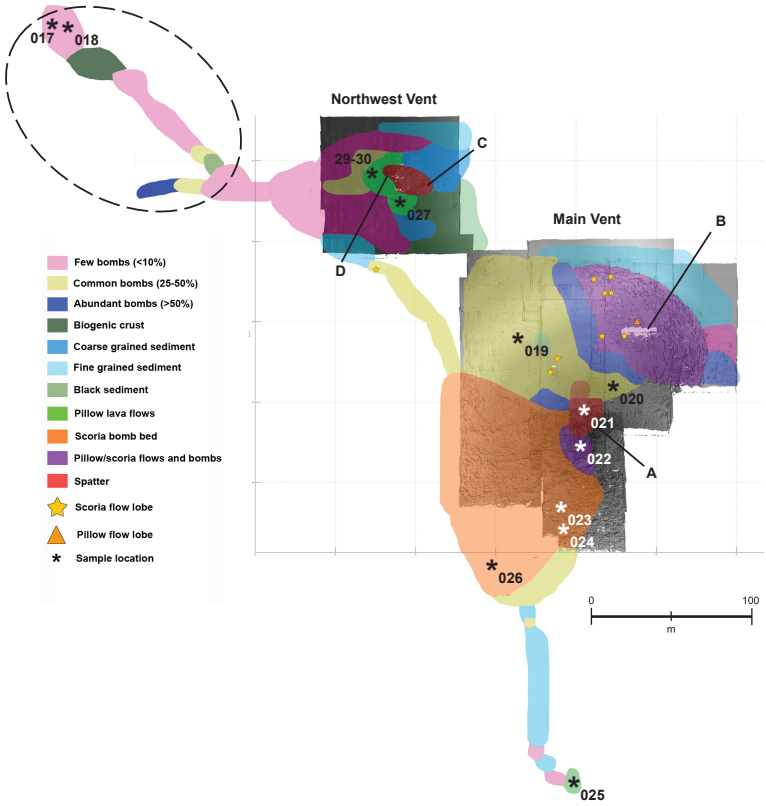

Fig. 11 Geologic map of the Foerstner and northwest vent sites. The dashed circle indicates the location of the sunken scoria balloons. Vent reference points A, B, C, D are shown in figures 10 and 11. Map was created using time stamped ROV video footage and Adobe Illustrator®.

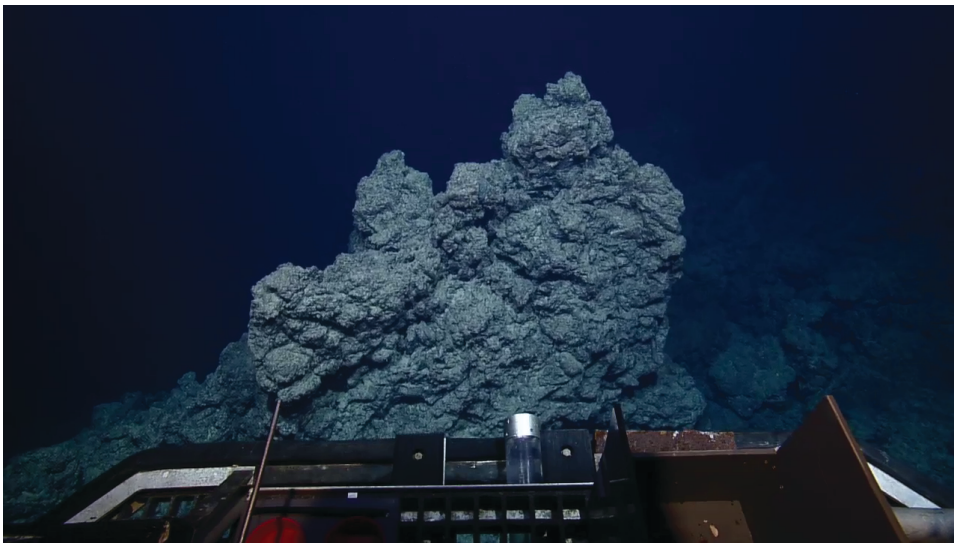

Fig. 12 Spatter-like deposits observed at the summits of both the Foerstner and northwest vent sites.

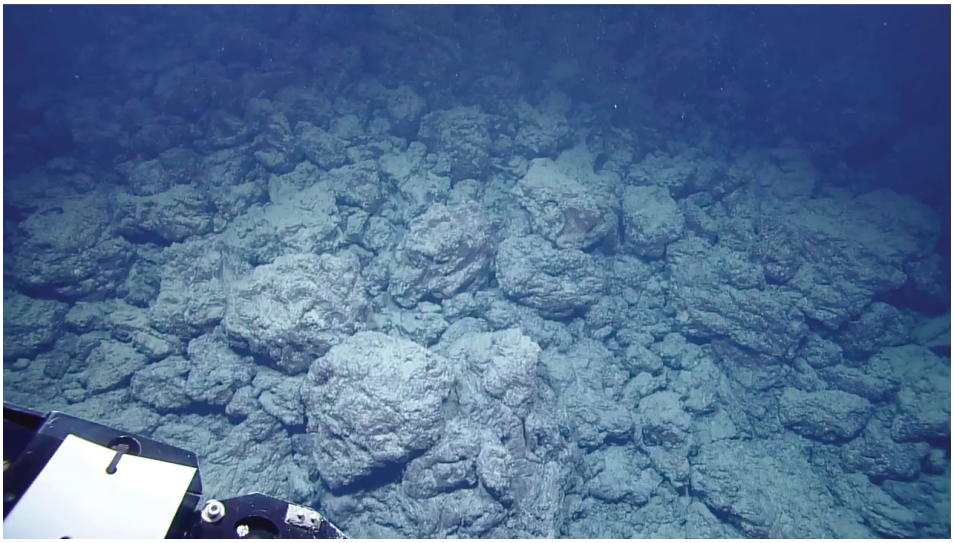

Fig. 13 Thick, clast-supported beds of coarse scoria bombs (scoria bomb bed).

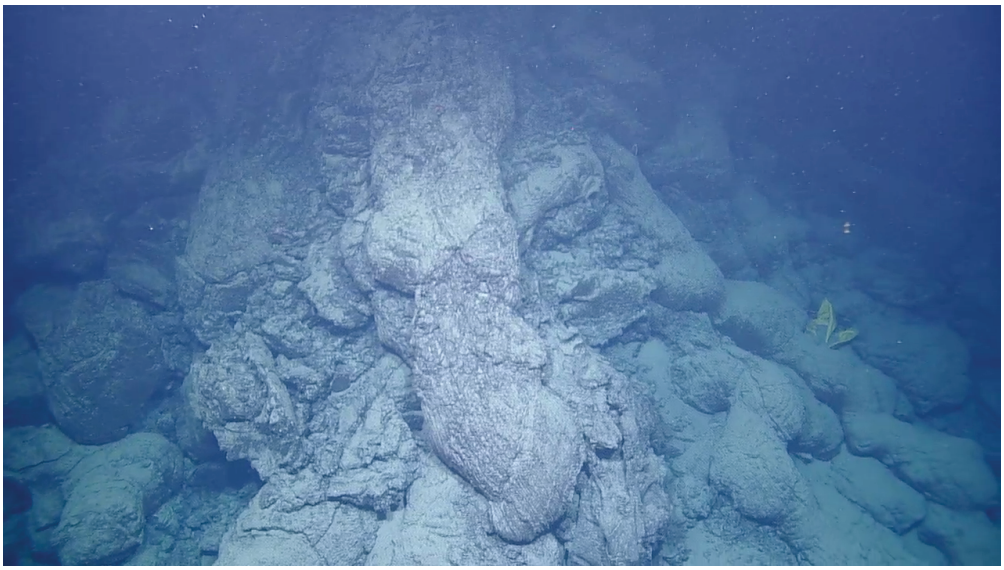

Fig. 14 Short, well defined pillow flows observed at the northwest and Foerstner vent sites.

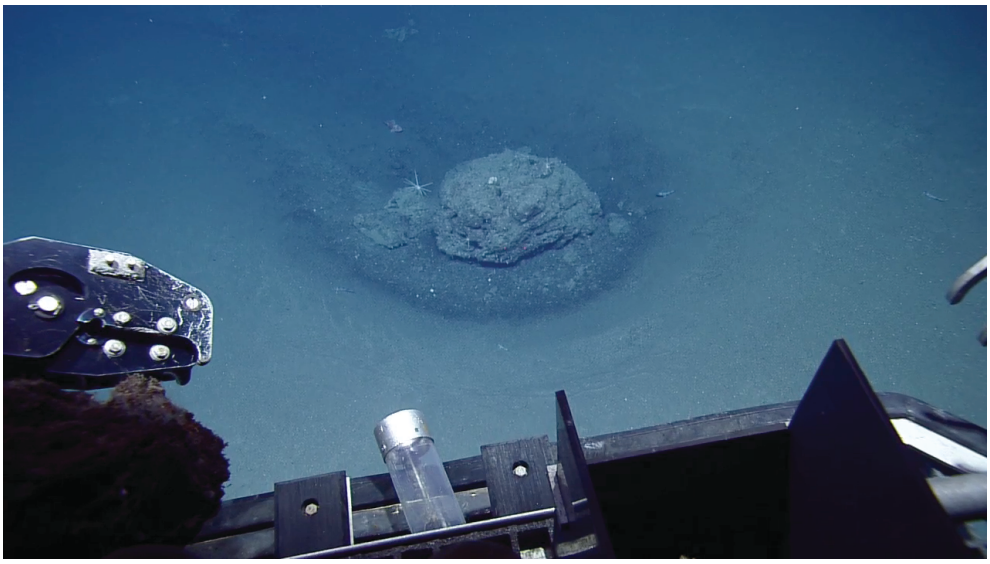

Fig. 15 Sunken scoria balloon bomb with its characteristic crater formed upon impact.

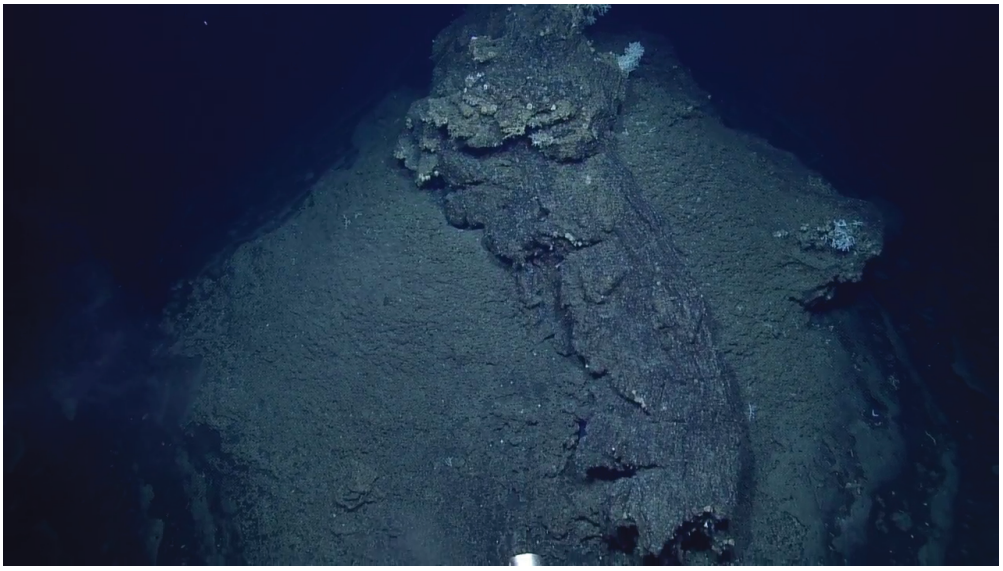

Fig. 16 Small, effusive vent discovered northwest of the small northwest mound constructed of a single detached scoria flow lobe.

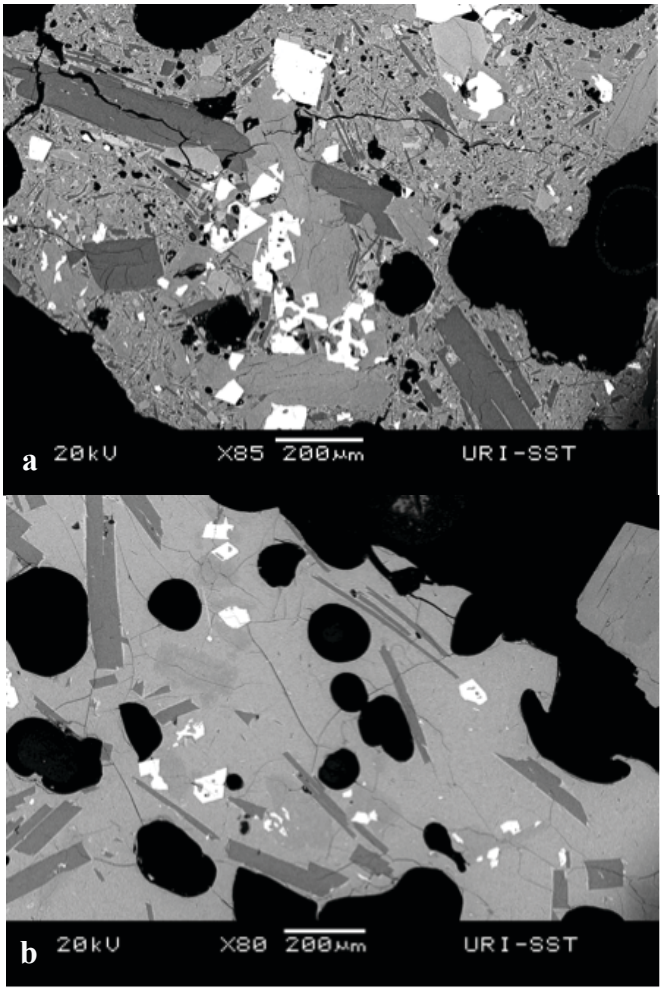

Fig. 17 Back-scattered electron (BSE) images of tachylite and sideromelane glass from the 1891 Foerstner eruption. **a** Cryptocrystalline texture of tachylite from sample NA018-021 **b** Hypocrystalline texture of sideromelane from sample NA018-027.

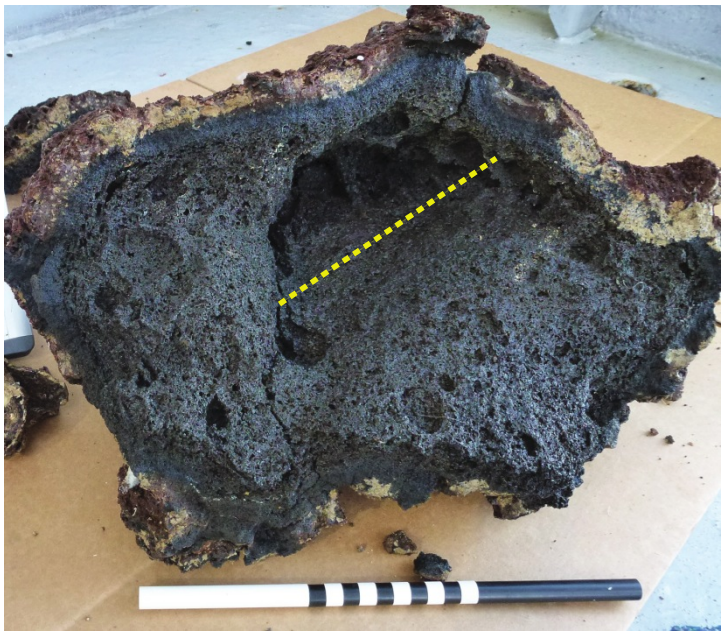

Fig. 18 Whole scoria balloon (NA018-18) looking into the interior (scale bar in cm). The dashed line indicates the extremely large internal vesicle.

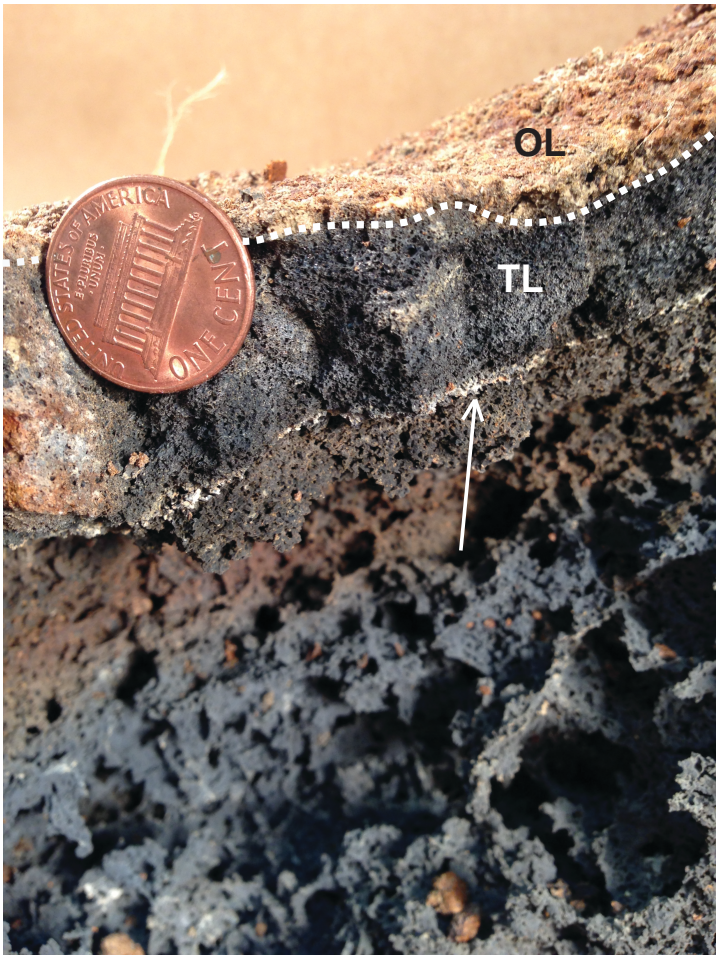

Fig. 19 Close up of the thin lava shell (NA018-18) showing the outer oxidized (OL) and inner tachylite (TL) layers labeled. Arrow points to the location of the white horizon layer separating the lava shell from the hollowed interior.

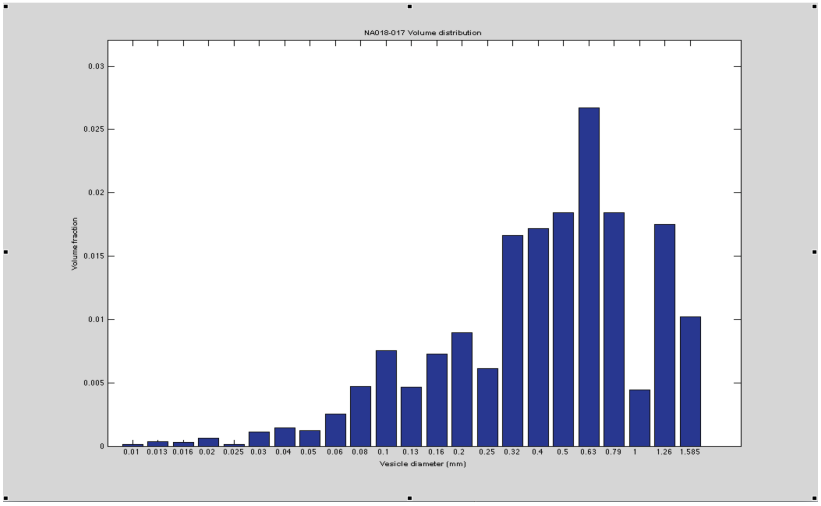

Fig. 20 Vesicle volume distribution (VVD) of a scoria balloon bomb recovered northwest of the northwest mound (NA018-017).

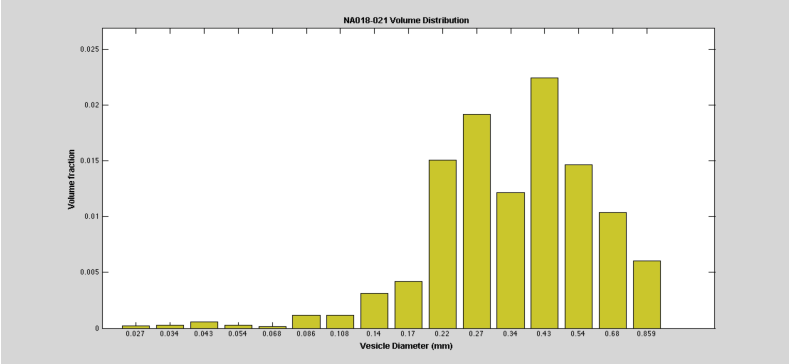

Fig. 21 Vesicle volume distribution (VVD) of a spatter-like deposit recovered from the summit of the main vent (NA018-021).

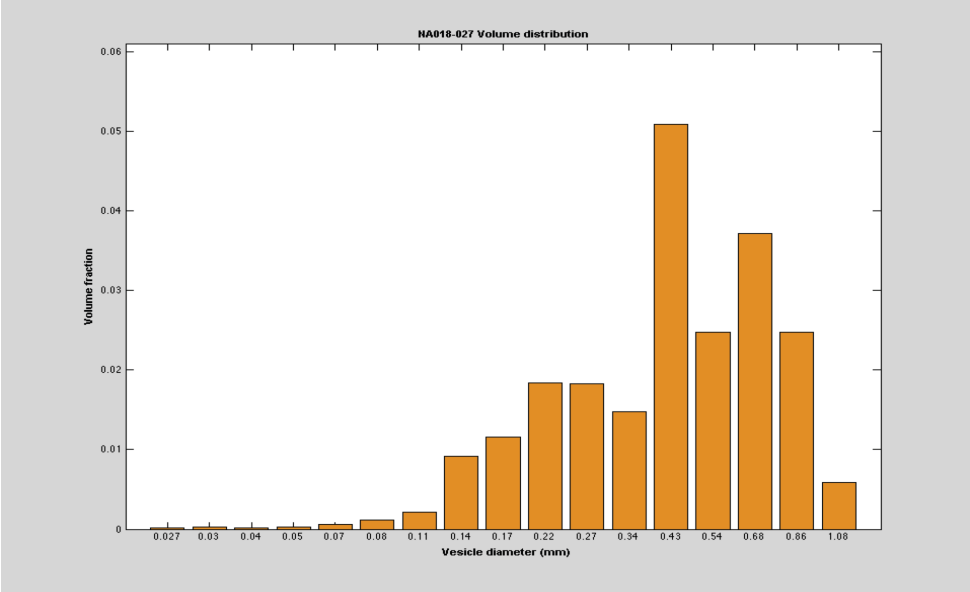

Fig. 22 Vesicle volume distribution of a pillow flow lobe fragment recovered from the northwest mound (NA018-027).

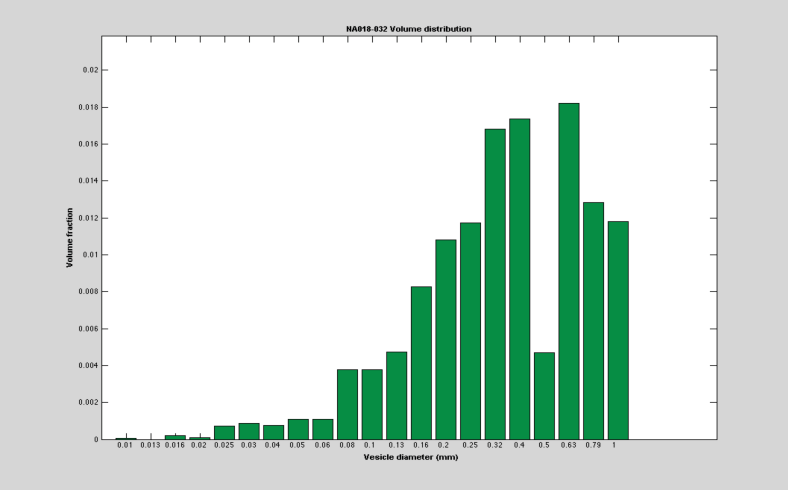

Fig. 23 Vesicle volume distribution of a scoria bomb representative of those observed at Foerstner recovered from the large western vent (NA018-032).